Immersion freezing of surface dust particles from Tengger Desert in China: effects of mineral composition and aging treatments on ice nucleating activity

Jiao Xue[1], Shengkai Wang[1], Haoyu Qi[1], Yao Yao[1], Shulan Chen[1], Yingjie Zhou[1], Juying Lu[1], Tian Zhang[1], Qi Wang[2], Defeng Zhao[3], Youwei Hong[4], Yihua Cai[1], Bingbing Wang[1,*]

[1]State Key Laboratory of Marine Environmental Science, College of Ocean and Earth Sciences, Xiamen University, Xiamen, China

[2]China-ASEAN College of Marine Sciences, Xiamen University Malaysia, Selangor Darul Ehsan, Malaysia

[3]Shanghai Key Laboratory of Ocean-land-atmosphere Boundary Dynamics and Climate Change, Fudan University, Shanghai, China

[4]School of Resource and Environmental Science, Quanzhou Normal University, Quanzhou, China

* *Corresponding authors:* Bingbing Wang (Bingbing.Wang@xmu.edu.cn)

Abstract

Mineral dust is a major source of ice nucleating particles (INPs) and thereby influences cloud properties, precipitation, and radiative forcing. However, the ice nucleation properties of natural dust and their response to atmospheric aging remain poorly constrained. Here, we investigated immersion freezing (IMF) of surface-collected dust from Tengger Desert, China, and examined the effects of internal mixing with ammonium sulfate (AS), NaCl, H_2SO_4, and HNO_3, as well as heat treatment. Median freezing temperature (T_{50}) of Tengger Desert dust increased from 253.6 to 258.5 K as dust mass fraction increased from 1.4×10^{-4} to 1.0×10^{-1} wt%. A minor increase in feldspar content (~2% in surface area) quantified by single particle analysis may contribute to the enhanced ice nucleation active site density (N_s). Internal mixing with AS enhanced IMF activity, with the enhancements of T_{50} (0.4 – 4.7 K), N_s, and heterogeneous ice nucleation rate coefficient (J_{het}) exhibiting sigmoidal response to AS concentration from 5×10^{-5} to 5×10^{-2} M. This sigmoidal response is consistent with a possible contribution from NH_4^+ adsorption on dust surface. NaCl and acids (H_2SO_4 and HNO_3), as well as heat treatment, had no impact on the overall IMF activity in terms of T_{50}, although modest changes in N_s were observed above 258 K. We developed experimentally constrained sensitivity parameterizations of N_s and J_{het} for Tengger Desert dust with and without aging, which may be used in cloud modeling to study how atmospheric aging modifies the ice nucleation of natural dust.

Keywords: Ice nucleation, single particle analysis, elemental composition, atmospheric aging, heat treatment

1. Introduction

Ice crystal formation is a fundamental atmospheric process that substantially modulate the microphysical properties and lifetime of cold clouds, precipitation, the Earth's radiation balance, and climate (Baker, 1997; Knopf and Alpert, 2023; Lohmann and Feichter, 2005; Rosenfeld et al., 2014; Storelvmo, 2017). Ice crystals may form via homogeneous or heterogeneous nucleation. Ice nucleating particles (INPs) reduce the free energy barrier for ice embryo formation and facilitate heterogeneous nucleation at lower relative humidity (RH) and higher temperatures than required for homogeneous nucleation (Pruppacher and Klett, 1997). Heterogeneous ice nucleation includes various pathways, including deposition nucleation, immersion freezing (IMF), condensation freezing, and contact freezing (Knopf et al., 2018; Ladino Moreno et al., 2013; Pruppacher and Klett, 1997; Vali et al., 2015). IMF is considered as the dominant heterogeneous nucleation mechanism in mixed-phase clouds (Kanji et al., 2017; Murray et al., 2012). Improved quantification of the IMF ability of diverse INP types is therefore critical for improving ice nucleation parameterizations and enhancing representations of aerosol-cloud interactions in cloud and climate models.

Mineral dust is a major INP class and contributes significantly to ice nucleation in mixed-phase clouds (Chen et al., 2024; DeMott et al., 2015; Hoose and Möhler, 2012; Kanji et al., 2017; Kawai et al., 2021; Ladino Moreno et al., 2013; Murray et al., 2012; Shi and Liu, 2019; Ullrich et al., 2017). Global model simulations indicate that the INP to dust mass ratio varies by an order of magnitude across dust source regions (Kawai and Matsui, 2025). Kawai et al. (2021) demonstrated that Asian dust contributes only 3.4% to global annual dust mass, yet accounts for more than 15% of global dust INPs. This disproportionate contribution is attributed to the long-range transport of Asian dust to the middle and upper troposphere for mixed-phase cloud formation. Despite this climatic implications, investigations on the ice nucleation properties of Asian dust are limited and often focus on particles collected during dust storms in urban environments. For instance, Zhao et al. (2024) found that dust from the 2021 Asian dust storms can

trigger IMF between 230 K and 250 K under water subsaturated conditions. Ice residual analysis conducted by Iwata and Matsuki (2018) showed that clay minerals dominated the ice active fraction above 243 K, whereas atmospheric aging (e.g., internal mixing with sea salt or nitrate coatings) suppressed ice nucleation. Chen et al. (2021) reported differences in IMF ability of particles during East Asian dust storms above 248 K linked to different desert regions and transport pathways. Li et al (2022) showed that surface dust/salt mixed particles from Chinese deserts can trigger deposition nucleation at temperatures as low as 223 K. Detailed investigations of IMF characteristics of Asian dust from source regions and the controlling factors are therefore required to accurately quantify their impacts on cloud formation.

Several studies have characterized the ice nucleating properties of natural dust from various source regions (Boose et al., 2016; Kaufmann et al., 2016; Perkins et al., 2020). Kaufmann et al. (2016) conducted ice nucleation measurement on dust from source regions on four continents and compared results with reference minerals, finding that natural dust froze within a narrow temperature range and that mineralogical composition can largely explained the freezing behavior for most samples. Boose et al. (2016) reported that the IMF ability of dust from nine typical deserts correlates with K-feldspar content at 253 K and with the abundance of feldspar and quartz between 238 K and 245K, whereas high clay content suppress IMF ability. Feldspar, particularly K-rich feldspar, is consistently identified as a highly ice active component that plays an important role in the freezing behavior of natural dust at high temperatures (e.g.，Atkinson et al., 2013; Harrison et al., 2016). Nevertheless, investigations on ice nucleation of natural dust from deserts remain limited relative to work on laboratory surrogate and monomineralic dust standards. Furthermore, the quantitative contributions by individual mineral components to ice nucleation activity of natural dust are not yet fully resolved.

Dust particles undergo atmospheric aging during long-range transport, including mixing with organics/inorganics and heterogeneous chemical reactions, which may

alter their intrinsic ice nucleation activity (Cziczo et al., 2013; DeMott et al., 2003; Eastwood et al., 2009; Kanji et al., 2013; Kulkarni et al., 2015; Möhler et al., 2008; Sullivan et al., 2010a, b; Tobo et al., 2012). Addition of soluble species (e.g., AS and NaCl) lowers water activity of aqueous droplets and thereby depresses freezing temperatures (Koop et al., 2000; Koop and Zobrist, 2009; Rigg et al., 2013; Zobrist et al., 2008). Emerging evidence indicates that low concentrations of certain solutes can modify the freezing temperature of dust via chemical interactions with ice active mineral components (Kumar et al., 2018, 2019a, b; Reischel and Vali, 1975; Whale et al., 2018; Wilson and Haymet, 2009; Worthy et al., 2021; Yun et al., 2021). For example, Whale et al. (2018) observed that ammonium salts increase the freezing temperature of feldspar and quartz, whereas NaCl reduces it. Similarly, Worthy et al. (2021) found that AS increases the freezing temperature of K-rich feldspar, kaolinite, montmorillonite, and Arizona Test Dust (ATD), which is attributed to NH_4^+/K^+ exchange and NH_4^+ adsorption that change interfacial water structure facilitating ice nucleation. In contrast, acid treatments diminish the IMF ability of feldspar, which is likely associated with H_3O^+/K^+ exchange and incongruent dissolution (Yun et al., 2021). Different aging treatments (acidic and salt solutions, peroxide, heating) have distinct effects on ice nucleation activity of ATD, underscoring the complexity of atmospheric processes (Niedermeier et al., 2011; Perkins et al., 2020).

Current studies have revealed diverse aging effects on the IMF ability of monomineralic particles and laboratory dust surrogates. Because of complex compositions of natural dust, results from simplified standards cannot be directly extrapolated to atmospheric dust. Consequently, the effects and mechanisms by which atmospheric aging alters the IMF of natural dust remain poorly constrained. Most aerosol-aware ice nucleation parameterizations generally distinguish broad particle types and relate freezing to temperature, humidity, particle abundance, or particle surface area (Burrows et al., 2022). However, they rarely represent atmospheric aging explicitly in regional and global models; when included, aging is treated with highly simplified assumptions.

Improved process-level constraints are therefore required to develop and evaluate the aging dependent ice nucleation parameterizations.

This study investigates the intrinsic IMF ability of natural dust from Tengger Desert and its response to different aging processes. We investigated the impacts on the IMF activity of surface-collected dust after heat treatment and mixing with AS, NaCl, H_2SO_4, and HNO_3. Single particle analysis provided size-resolved elemental compositions and quantified the contribution of mineral components. We quantify changes in IMF ability of dust induced by each aging treatment, discuss plausible mechanisms, and propose corresponding ice nucleation parameterizations with potential atmospheric implication.

2 Experimental methods

2.1 Sample collection and preparation

Surface dust particles were collected from the Tengger Desert, China (37.57°N,104.93°E) (Fig. 1). The experimental procedure is summarized in Fig. 2. Dust particles was sieved (200 mesh, 74 μm, nylon) and used for suspension preparation. A weighed dust aliquot was mixed with 20 mL ultrapure water (Millipore, resistivity > 18.2 MΩ cm) in a glass vial and manually shaken for 1-2 minutes to ensure thorough mixing. After standing for 5 min to allow coarse particles to settle, the upper 10 mL was collected as the first dust suspension (hereafter referred as S-dust). A second suspension was prepared using the same procedure but subjected to ultrasonic treatment at 40 kHz for 30 min at 25 °C in an ultrasonic bath (KQ2200DA, Kunshan Ultrasonic Instrument Ltd.). This sample is hereafter referred to as ultrasonicated dust (Us-dust). The sonication duration was selected based on Knopf and Alpert (2013) to reduce particle aggregation and promote the dispersion of fine dust particles in the 20 mL suspension. The upper portion (~10 mL) of each 20 mL dust suspension was collected and serially diluted with ultrapure for immediate used in the ice nucleation experiments. To determine dust mass concentration, 6 mL of each suspension was filtered using 0.2 μm polycarbonate filter membrane (GTTP04700, Isopore^{TM}) and the insoluble part was weighed. Ultrasonic treatment increased the dust mass concentration in suspension by

about 5 times. The following suspensions were used. For S-dust, the mass concentrations were 2.0×10^{-2} wt%, 3.0×10^{-3} wt%, and 7.0×10^{-4} wt%. The mass concentrations for Us-dust were 1.0×10^{-1} wt%, 1.87×10^{-2} wt%, 3.5×10^{-3} wt%, 7.0×10^{-4} wt%, and 1.4×10^{-4} wt%.

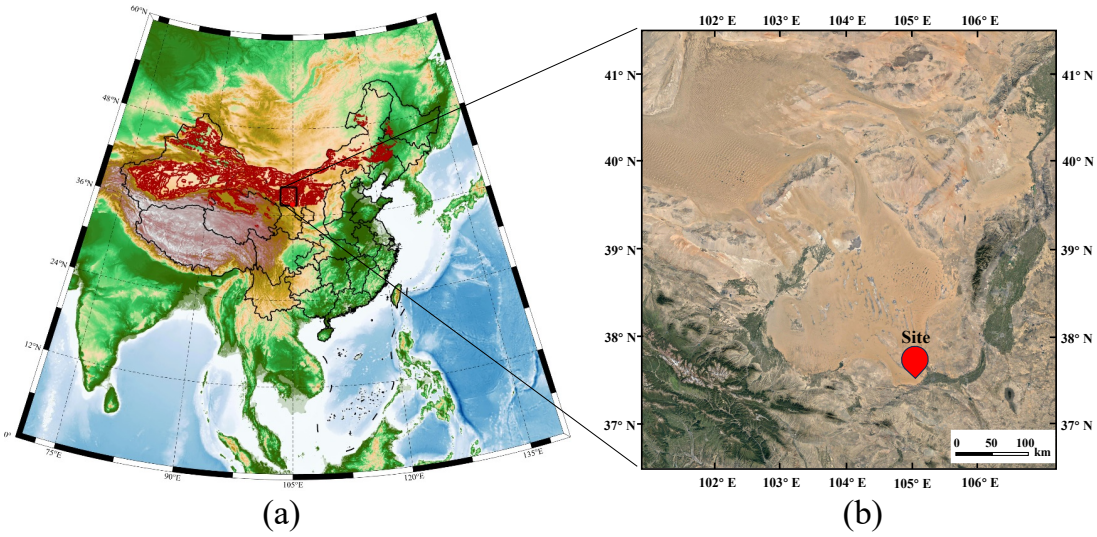

Figure 1. (a) Deserts in northern China (red shading) and the location of Tengger desert (black rectangle). (b) Sampling site (red dot) in Tengger Desert (Map data © 2026 Google)

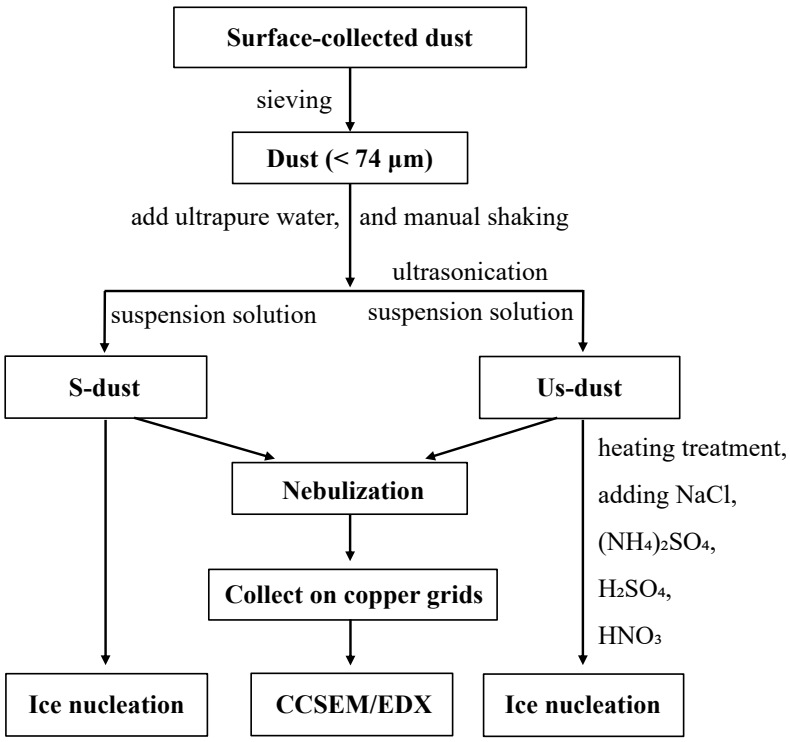

Figure 2. Schematic diagram of experimental procedures.

2.2 Aging treatments on Us-dust

All aging treatments used the Us-dust suspension with dust mass concentration of 1.87×10^{-2} wt%. We added AS, NaCl, HNO_3, and H_2SO_4 to the Us-dust suspension for 12 hours prior to ice nucleation experiments. Final AS concentrations (99.95%, Sigma) were 5×10^{-5} M, 5×10^{-4} M, 5×10^{-3} M, 2×10^{-3} M, 1×10^{-3} M, and 5×10^{-2} M. Final NaCl concentrations (99.995%, Sigma) were 5×10^{-4} M, 5×10^{-3} M, 5×10^{-2} M. Final H_2SO_4 concentrations (99.7%, Hushi) were 2.5×10^{-4} M, 2.5×10^{-3} M, 2.5×10^{-2} M. Final HNO_3 concentrations (99.7%, Hushi) were 5×10^{-4} M, 5×10^{-3} M, 5×10^{-2} M. Heat treatment was conducted on the Us-dust suspension at 95 °C for 30 min.

2.3 Size-resolved composition of dust particles

Single particle analysis was conducted by the computer-controlled scanning electron microscopy equipped with an energy dispersive X-ray spectroscopy (CCSEM/EDX, Quanta 650, FEI Inc.; Genesis, EDAX Inc.) to determine particle size and elemental composition. Dust particles were collected from the suspensions following the method from our previous work (Xue et al., 2024; Zhao et al., 2024). Briefly, the upper portion (~10 mL) of each 20 mL dust suspension was nebulized. The generated aerosols were carried by high-purity nitrogen through a diffusion dryer and collected onto TEM copper grids (01814-F, Ted Pella) using an impactor (SKC, Inc.). CCSEM/EDX analysis at the working voltage of 20 kV followed the established method from our previous work (Knopf et al., 2014; Laskin et al., 2002; Wang et al., 2012; Xue et al., 2024; Zhao et al., 2024) and is described briefly here. The elemental composition and the area equipment dimeter (calculated by the 2-D projected particle area, hereafter referred as particle size) were quantified for about 1040 S-dust and 1180 Us-dust particles. We obtained atomic percentages for C, N, O, Na, Mg, Al, Si, P, Si, Cl, K, Ca, and Fe. C, N, and O determined by EDX were semiquantitative and excluded from classification. For each particle, the normalized atomic percentage of element X was calculated as $[X] = \frac{X}{Na+Mg+Al+Si+K+Ca+Fe+P+S+Cl}$. Based on the elemental

composition, particles were grouped into five types, namely illite, kaolinite, chlorite, quartz, and feldspar, using a rule-based classification scheme (Fig. 3). This method has been widely used to identify different dust types based on the elemental fingerprints of monomineralic dust (Hu et al., 2022; Kandler et al., 2007; Wang et al., 2022; Zhao et al., 2024). Mean elemental compositions of each dust type were shown in Fig. S1.

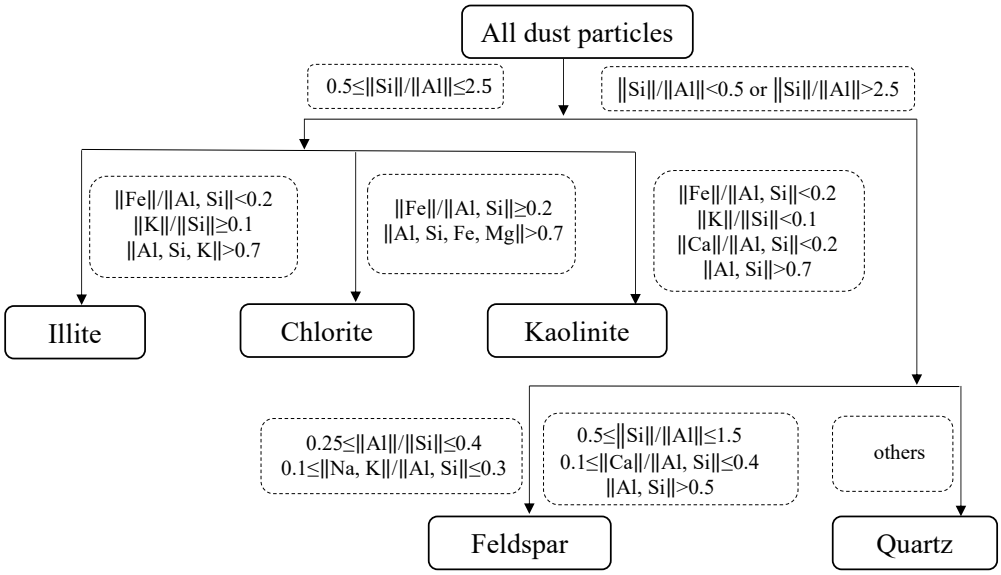

Figure 3. Particle classification scheme based on the relative atomic percentages of elements obtained from CCSEM/EDX analysis of individual particles.

2.4 Immersion freezing experiments

IMF experiments were performed using a temperature-controlled cooling stage coupled to an optical microscope, following the method described by Knopf and Forrester (2011) and Yao et al. (2023). About 20-25 of 1 μL droplets (dust suspensions or ultrapure water) were pipetted onto a hydrophobic glass slide, covered with a second hydrophobic glass slide and a custom copper spacer, and sealed with vacuum grease to isolate the droplets from ambient environment. The sample cell was placed on the cooling stage for subsequent freezing experiment. Sample temperature was regulated by circulating liquid nitrogen through the cooling stage and a heating foil under feedback from a temperature controller. Droplet temperature was calibrated against the melting points of decane and dodecane and a conservative temperature uncertainty was estimated to

be ± 0.5 K (Text S1 and Fig. S2). Freezing experiment was conducted at 10 K min^{-1} while a digital camera recorded the freezing process at one picture per second. The cooling rate of 10 K min^{-1} was selected following previous studies (Knopf and Lopez, 2009; Koop et al., 1998) to reduce the time available for water vapor transfer between supercooled droplets and ice crystals and minimize potential interference from the Bergeron–Wegener–Findeisen process. At least three independent samples were measured, each with more than three repeated runs, yielding about 200 – 270 freezing events per droplet type. Freezing temperature of each droplet was determined by analyzing the recorded images. Ultrapure water droplets (resistivity > 18.2 MΩ cm) served as background. The freezing temperatures were corrected for freezing point depression induced by solutes (ΔT_f), which was calculated as follows:

$$\Delta T_{\mathrm{f}} = i \times K_{\mathrm{f}} \times m_{solute}, \quad (1)$$

where i is van't Hoff factor, K_f is cryoscopic constant (1.86 K kg mol^{-1}), and m_{solute} is solute molality (Worthy et al., 2021).

Additional freezing experiments were conducted using water droplets and Tengger Desert dust suspensions at different cooling rates (Text S1 and Fig. S3). T_{50} showed little variation at cooling rate between 0.5 and 2 K min^{-1}, whereas the difference in T_{50} between 10 and 1 K min^{-1} were +1.1 K at 255 K and -0.9 K at 245 K. These differences may partly reflect the cooling rate effect due to the time dependent nature of nucleation, although this effect varies among ice nucleating materials and with particle surface area (Broadley et al., 2012; Murray et al., 2011, 2012; Wright et al., 2013). Potential contributions to these differences from temperature uncertainties cannot be excluded.

2.5 Frozen fraction and ice nucleating active site density

Frozen fraction ($f_{ice}(T)$) is defined as the ratio of the number of frozen droplets (N_{ice}) at a certain temperature (T) to the total number of droplets (N_{total}), i.e., $f_{\mathrm{ice}}(T) = N_{\mathrm{ice}}/N_{\mathrm{total}}$. Frozen fraction reflects the distribution of ice formation event at different temperatures. Ice nucleation active site density (N_s) is the number of ice active site per unit particle surface area and is calculated using Eq. (2) according to Vali (1971):

$$N_s = \frac{-\ln\left(1 - f_{ice}(T)\right)}{A} \quad [m^{-2}] \tag{2}$$

where A is the total particle surface area immersed in a single droplet. A was calculated by the particle mass in the droplet and the average surface area per unit particle mass (A_m). Particle mass in each droplet equals the dust mass concentration in suspension times the droplet volume (1 μL). A_m was estimated from CCSEM/EDX particle data by

$$A_m = \frac{\sum S_i}{\sum V_i \times \rho_i} \tag{3}$$

where S_i is the surface area of the individual particle i (assumed spherical, $S_i = \pi {d_i}^2$); V_i is the volume of the individual particle i, $V_i = \pi {d_i}^3/6$; d_i is the diameter of the particle i; ρ_i is the density of different particle types, specifically, ρ_{quartz} = 2.62 g cm^{-3}, $\rho_{chlorite}$ = 2.42 g cm^{-3}, ρ_{illite} = 2.6 g cm^{-3}, $\rho_{kaolinite}$ = 2.6 g cm^{-3}, and $\rho_{feldspar}$ = 2.6 g cm^{-3} (Menut et al., 2020). Uncertainty in N_s (95% confidence intervals) was calculated using Poisson nucleation statistics (Koop et al., 1997).

2.6 Heterogeneous ice nucleation rate coefficient (J_{het})

Experimental data were used to derive J_{het}, providing a time-dependent description of heterogeneous nucleation. J_{het} at temperature T^i for a given temperature interval (ΔT) was calculated based on the method from previous studies (Alpert et al., 2011; Koop et al., 1997; Zobrist et al., 2007):

$$J_{\text{het}}\left(T^i\right) = \frac{N_{\text{ice}}^i}{t_{\text{tot}}^i \times A^i} \tag{4}$$

where N_{ice}^i is the total number of ice nucleation events in the ith temperature interval, and $t_{\text{tot}}^i \times A^i$ is product of observation time and dust surface area available for nucleation in that interval. $t_{\text{tot}}^i \times A^i$ is given by

$$t_{\text{tot}}^i \times A^i = \sum_{j=1}^{N_{\text{ice}}^i} \frac{\left(T_{\text{st}}^i - T_{\text{ice},j}^i\right)}{c_{\text{r}}} A_{liq,j}^i + \frac{\Delta T}{c_{\text{r}}} A_{liq}^i \tag{5}$$

where T_{st}^i is the start temperature of ith temperature interval; $T_{\text{ice},j}^i$ and $A_{liq,j}^i$ are the freezing temperature and dust surface area of the jth droplet that froze within the interval; A_{liq}^i is the total dust surface area in the droplets remaining liquid at the end of the

interval; c_r is the cooling rate (10 K min^{-1}); ΔT of 0.5 K is used.

The experimentally derived J_{het} was parameterized using the water activity based framework which relates the droplet freezing temperature uniquely to droplet water activity (Alpert et al., 2022; Knopf and Alpert, 2013; Xue et al., 2024; Zhao et al., 2024). It has been applied to both homogeneous and heterogeneous ice nucleation (China et al., 2017; Knopf and Alpert, 2013; Koop and Zobrist, 2009). In this framework, Δa_w is used to describe the freezing ability of droplets, which represents the deviation of the water activity of droplets at freezing temperature from the water activity at the ice-melting equilibrium state at the same temperature (Koop et al., 2000). Δa_w was calculated for each droplet at its freezing temperature. The corresponding J_{het} was parameterized by a liner regression of log (J_{het}) against Δa_w (or temperature). Note that the derived J_{het} values reported in this study correspond to a cooling rate of 10 K min^{-1}; therefore, comparisons with studies using different cooling rates should be made with caution.

The surface area used to calculate N_s and J_{het} and was estimated from the geometric particle diameters measured by CCSEM/EDX, rather than Brunauer-Emmett-Teller (BET) specific surface area. Because these methods quantify different surface area metrics, comparisons with literature N_s and J_{het} values or parameterizations based on BET surface area should be made cautiously. Dynamic light scattering (DLS) measurements were performed to independently assess the particle size distribution in the suspensions and estimate the geometric surface area per 1 μL droplet (Text S2 and Fig. S4). The DLS- and CCSEM-derived surface area estimates were within the same order of magnitude, although the latter were approximately 2-3 times higher.

3 Results and discussion

3.1 Characteristics of Tengger Desert dust at single particle level

Figure 4 shows the particle classification for the S-dust and Us-dust samples. Particles were mainly in the size range of 0.2-2 μm. S-dust and Us-dust exhibited a peak size of about 0.35 μm and 0.7 μm, respectively. Size distributions of the same particle type between S-dust and Us-dust were slightly different (Fig. 4b, f). Particle number

contribution of Us-dust by kaolinite, quartz, illite, chlorite, and feldspar was 32%, 29%, 19%, 12%, and 7%, respectively. Compared with S-dust, chlorite, illite, and feldspar in Us-dust is about 12%, 11%, and 2% higher, respectively, whereas kaolinite decreased by 23% and quartz remained unchanged (Fig. 4c, g). The contribution to particle surface area of Us-dust by illite, quartz, chlorite, kaolinite, and feldspar was 37%, 24%, 23%, 12%, and 5%, respectively. Compared with S-dust, Us-dust showed higher contributions from chlorite (13%), illite (4%), and feldspar (2%), and lower contributions from quartz (3%) and kaolinite (15%) (Fig. 4d, h).

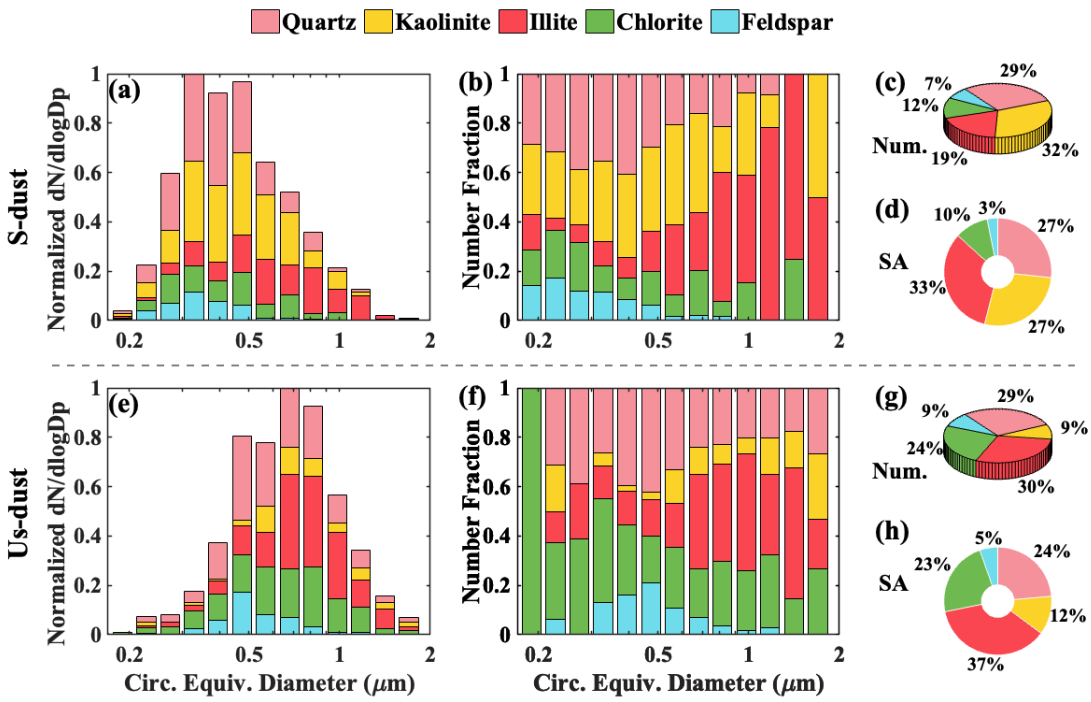

Figure 4. Particle size distribution and contribution of dust types for S-dust (upper panel, a-d) and Us-dust (lower panel, e-h). Normalized particle size distribution (a, e); relative number fraction of each particle type as a function of size (b, f); the number (c, g) and surface area (d, h) contribution of each particle type.

3.2 Ice nucleation ability of Tengger Desert dust

Figure 5 summarizes IMF experimental results for ultrapure water droplets and dust-containing droplets. Both S-dust and Us-dust at the investigated concentrations induced IMF at higher temperatures than water droplets (Fig. 5a). T_{50} changed from 252.4 K to 254.6 K for S-dust as concentration increased from 7.0×10^{-4} wt% to 2.0×10^{-2} wt%. T_{50}

changed from 253.6 K to 258.5 K for Us-dust as concentration rose from 1.4×10^{-4} wt% to 1.0×10^{-1} wt%. T_{50} shows that Us-dust nucleated ice more efficient than S-dust (Fig. 5b). At comparable dust surface area concentration, T_{50} of Us-dust was about 2 K higher than S-dust. T_{50} increased by about 1.1 K and 1.2 K per decade increase in dust surface area concentration for S-dust and Us-dust, respectively. We defined ΔT_{50}^{w}, as the T_{50} difference between dust-containing droplets and water droplets. Figure 5c compares the ΔT_{50}^{w} for S-dust, Us-dust, and other monomineralic dust. ΔT_{50}^{w} of monomineralic dust ranks as follows: K-feldspar > Na/Ca-feldspar > quartz > illite > kaolinite > chlorite. T_{50}^{w} for Us-dust was consistent with Na/Ca-feldspar but low than K-feldspar, while ΔT_{50}^{w} for S-dust was lower than Na/Ca-feldspar, but higher than chlorite and illite. We have shown that the contributions of chlorite, illite, and feldspar in both number and surface area were higher in Us-dust compared to S-dust (Fig. 4). Given that the ΔT_{50}^{w} of chlorite and illite are lower than U-dust, the improved IMF ability of Us-dust relative to S-dust may be partly attributed to the increased feldspar content.

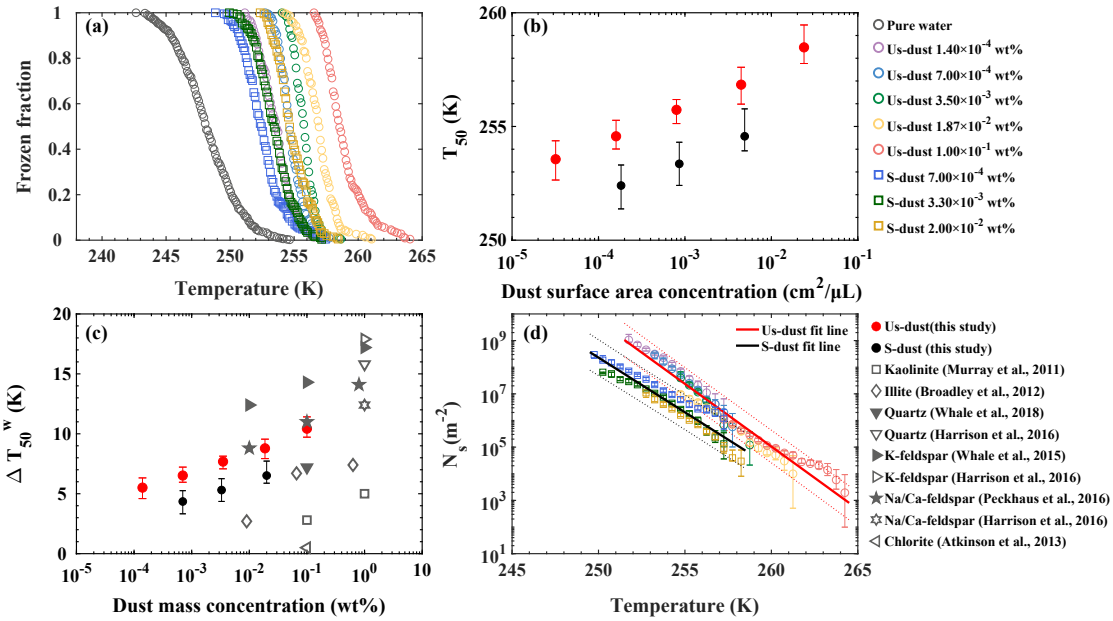

Figure 5. (a) Frozen fraction of water droplets, Us-dust and S-dust containing droplets. (b) T_{50} as a function of dust surface area concentration within a droplet. (c) ΔT_{50}^{w} as a function of dust mass concentration. Error bars (b, c) in temperature correspond to the 25th and 75th percentiles of freezing temperature. Gray symbols (c) represent monomineralic dust from previous studies (Atkinson et al., 2013; Broadley et al., 2012; Harrison et al., 2016; Murray et al., 2011;

Peckhaus et al., 2016; Whale et al., 2015, 2018). (d) N_s as a function of temperature. Error bars for N_s correspond to the 95% confidence intervals. Black and red lines were fitted lines for Us-dust and S-dust, respectively. Dotted lines indicate the 95% prediction intervals.

Figure 5d shows the N_s for S-dust and Us-dust with parameterizations using the function of $log_{10}(N_s) = m_1 \times T + n_1$. The values of m_1 and n_1 are shown in Table 1. Overall, N_s for Us-dust was about one order of magnitude higher than S-dust. As shown in Fig. 6a, N_s for Us-dust was comparable to feldspar, falling in between Na/Ca-feldspar and K-feldspar. The N_s of S-dust was similar to Na-feldspar, and was distinctly higher than quartz, illite and chlorite. Previous studies has suggested that K-feldspar may enhance the ice nucleation activity (Boose et al., 2019; Harrison et al., 2016). Notably, both Us-dust and S-dust showed stronger temperature dependences of N_s than previously reported N_s for ATD, natural dust from deserts, and airborne particles during dust storms (Chen et al., 2021; Hader et al., 2014; Niemand et al., 2012; Reicher et al., 2019; Ullrich et al., 2017). Us-dust and S-dust exhibited N_s similar to those airborne particles collected during dust storms below 260 K, but lower N_s above 260 K (Fig. 6b). However, N_s for Tengger desert dust was lower than the N_s parameterizations reported by Niemand et al. (2012) and Ullrich et al. (2017), especially at high temperatures. This observed discrepancy in N_s is likely attributed to the differences in particle size and composition of these surface-collected or airborne dust particles. Additionally, atmospheric aging on dust during long-range transport may also contribute to the discrepancy.

Table 1 The m_1 and n_1 values for the N_s parameterizations of Tengger Desert dust as a function of temperature (T), $\log(N_s) = m_1 \times T + n_1$

Samples	m_1	LCL_{m1}	UCL_{m1}	n_1	LCL_{n1}	UCL_{n1}	***RMSE***	R^2
Us-dust	-0.47	-0.50	-0.44	127.31	120.45	134.18	0.30	0.96
S-dust	-0.41	-0.45	-0.37	111.03	100.09	121.98	0.32	0.90

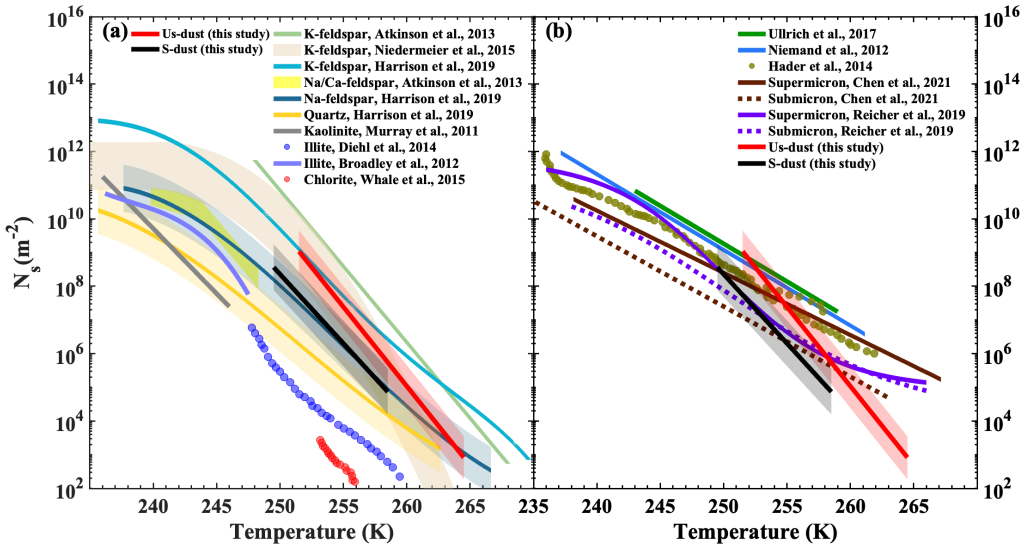

Figure 6. (a) Comparison of N_s parameterizations for Us-dust, S-dust, and monomineralic dusts from previous studies (Atkinson et al., 2013; Broadley et al., 2012; Diehl et al., 2014; Harrison et al., 2016; Murray et al., 2011; Niedermeier et al., 2011; Whale et al., 2015). Shade areas of N_s for Us-dust and S-dust are the 95% prediction intervals. (b) Comparison of N_s parameterizations for Us-dust, S-dust, ATD (Hader et al., 2014), soil samples, desert dust, and airborne dust (Chen et al., 2021; Niemand et al., 2012; Reicher et al., 2019; Ullrich et al., 2017). The detail sample information for each parameterization is shown in Table S1.

3.3 Ice nucleation ability of dust mixed with ammonium sulfate

Figure 7 presents the IMF results for Us-dust at 1.87×10^{-2} wt% after mixing with AS at various concentrations. AS enhanced the IMF ability of Us-dust, leading to higher freezing temperature and N_s as AS concentration increases (Fig. 7a, b). At AS concentration above 5×10^{-3} M, N_s was approximately two orders of magnitude larger than untreated Us-dust. We define ΔT_{50}^{u} as the T_{50} difference between AS treated and untreated Us-dust, using T_{50} of 256.8 K for the untreated Us-dust at 1.87×10^{-2} wt%. ΔT_{50}^{u} increased from 0.4 K to 4.7 K as AS concentration increased from 5×10^{-5} M to 5×10^{-2} M (Fig. 7c), following a sigmoidal response reproduced via a Boltzmann function as:

$$\Delta T_{50}^{u} = 0.3997 + 4.2685/\left(1 + exp\left((\log_{10}[AS] + 3.0324)/-0.2845\right)\right) \quad (6).$$

Previous studies have suggested that the interaction between dust and ammonium ions

(NH_4^+) can enhance the IMF ability of dust (Anim-Danso et al., 2016; Kumar et al., 2018; Whale et al., 2018; Worthy et al., 2021). The observed sigmoidal response of ΔT_{50}^{u} suggests a concentration dependent activation of ice nucleation sites on dust surface upon AS exposure. At relatively at low AS concentration down to 5×10^{-5} M, the enhancement was modest, with a ΔT_{50}^{u} of 0.4 K, suggesting that only a small fraction of susceptible ice nucleation sites was activated. As the AS concentration increased to 5×10^{-3} M, ΔT_{50}^{u} increased markedly to 4.7 K, consistent with a substantial activation of additional ice nucleation sites. At a higher AS concentration of 5×10^{-2} M, ΔT_{50}^{u} remained nearly constant, suggesting that the enhancement had approached a plateau. One possible explanation is that most of the susceptible ice nucleation sites had already been activated, potentially reflecting saturation of the relevant surface interactions involving NH_4^+. This interpretation is consistent with the proposed role of ammonium–dust interactions in enhancing ice nucleation, although the underlying molecular mechanism remains to be confirmed. Further discussion is provided in Section 3.5.1.

ΔT_{50}^{u} for Us-dust mixed with AS fell within the upper range reported for other minerals (Fig.7c). At AS concentrations of 10^{-4} M – 10^{-3} M, Us-dust exhibited comparable ΔT_{50}^{u} to K-feldspar, but was greater at higher AS concentrations than those reported by Whale et al. (2018) and Worthy et al. (2021). To eliminate biases originating from inconsistent dust concentrations in these studies, AS content was normalized by dust concentration and expressed as the mass ratio of AS to dust (AS/Dust) for intercomparison (Fig. 7d). ΔT_{50}^{u} increased with AS/Dust ratio with a more pronounced sigmoidal shape, which is fitted by a Boltzmann function as:

$$\Delta T_{50}^{u} = 0.3998 + 4.2682/\left(1 + exp\left((\log_{10}(AS/Dust) + 0.1837)/-0.2844\right)\right) \quad (7).$$

When plotted against AS/Dust, ΔT_{50}^{u} for Us-dust generally converges to the range of ΔT_{50}^{u} for K-feldspar (Whale et al., 2018; Worthy et al., 2021). However, ΔT_{50}^{u} for K-feldspar tended to be a linear response against either log values of AS concentration or AS/Dust ratios. ΔT_{50}^{u} for Us-dust was greater than quartz but lower than kaolinite at the investigated AS concentrations. ΔT_{50}^{u} for Us-dust was slightly lower than ATD reported by Worthy et al. (2021), but higher than ATD from Whale et al. (2018). These

differences in ΔT_{50}^{u} or its trend was likely controlled by divergent interfacial interactions between AS and various minerals of the investigated dust. In addition, Worthy et al. (2021) suggested that those inconsistencies may be associated with the different contact time between AS and dust.

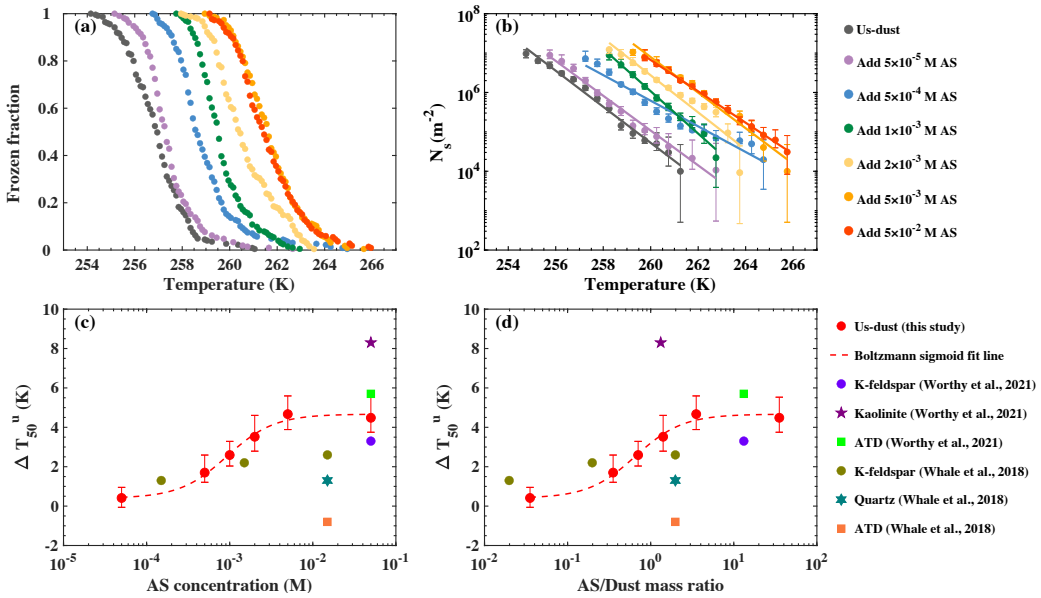

Figure 7. (a) Frozen fraction for Us-dust (1.87×10^{-2} wt%) mixed with ammonium sulfate (AS) at different concentrations. (b) N_s with error bars corresponding to the 95% confidence intervals. Solid lines are parameterizations of N_s. (c) ΔT_{50}^{u} as a function of AS concentration. (d) ΔT_{50}^{u} as a function of the mass ratio of AS to dust (AS/Dust). Dashed lines (c, d) represent the Boltzmann sigmoid fitting. Error bars (c, d) represent the 25% and 75% percentiles. The literature data in panels (c) and (d) are from Whale et al. (2018) and Worthy et al. (2021).

3.4 Ice nucleation ability of dust mixed with NaCl or acids and after heating

Figure 8 shows that ΔT_{50}^{u} for Us-dust were close to zero after heat treatment, mixed with NaCl, or acid (H_2SO_4 or HNO_3) treatment. This indicates that these treatments had no impacts on IMF ability of Us-dust when comparing the T_{50} values. However, these treatments had certain effects on the IMF ability at freezing temperature above 258 K as evidenced by the deviations in N_s (Fig. 8d-f) and frozen fraction (Fig. S5). Specifically, heat and H_2SO_4 treatments, as well as higher concentrations of NaCl (5×10^{-2} M) and HNO_3 (2.5×10^{-2} M) treatments imposed a reduction in N_s, whereas

lower concentrations of NaCl (5×10^{-4} M) and HNO_3 (5×10^{-4} M and 5×10^{-3} M) treatments led to an increase in N_s. The impact of heat treatment on Us-dust was qualitatively consistent with the results from Zolles et al (2015), who reported marginal change in the IMF ability of K-feldspar, Na/Ca-feldspar, Kaolinite, and ATD after heating at 523 K for 4-5 h, with the ΔT_{50}^{u} values remaining within their measurement uncertainty.

Previous studies show that NaCl and acids can reduce the IMF ability of K-feldspar, kaolinite, and quartz (Reischel and Vali, 1975; Whale, 2022; Whale et al., 2018; Yun et al., 2021) (Fig. 8a, b). For K-feldspar and kaolinite, higher NaCl concentration led to lower ΔT_{50}^{u} (negative values). Higher HCl and HNO_3 concentrations led to a stronger reduction in ΔT_{50}^{u} for K-feldspar (Reischel and Vali, 1975; Whale et al., 2018). However, NaCl and HCl did not affect the IMF ability of ATD (Link et al., 2020; Perkins et al., 2020), which was similar to Us-dust. Although, NaCl, heat, and acid treatments did not substantially change the T_{50} of Us-dust, they altered N_s leading to the enhancement or reduction in the IMF ability of Us-dust at warmer freezing temperature. A similar phenomenon was also observed for ATD when mixed with inorganic acids (Perkins et al., 2020).

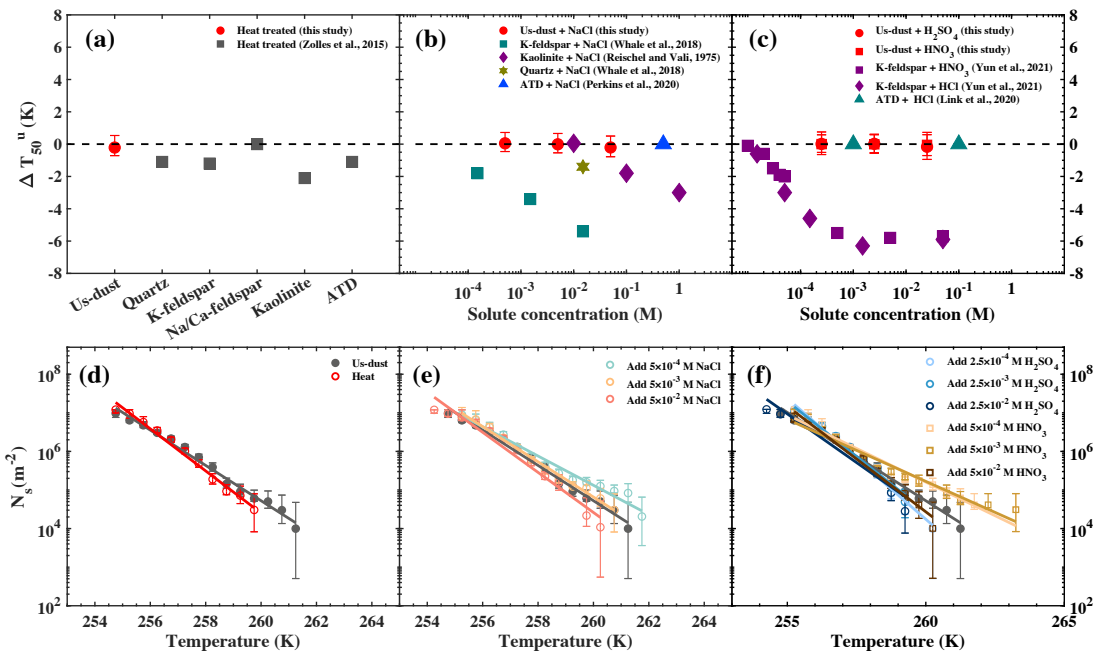

Figure 8. Comparison of ΔT_{50}^{u} (a-c) and N_s (d-f) for Us-dust treated by heating, adding NaCl,

H_2SO_4 and HNO_3. Error bars for ΔT_{50}^{u} represent the 25% and 75% percentiles. Error bars for N_s correspond to the 95% confidence intervals. Solid lines are parameterizations of N_s. The comparison data in panels (a, b, c) are from previous studies (Link et al., 2020; Perkins et al., 2020; Reischel and Vali, 1975; Whale et al., 2018; Yun et al., 2021; Zolles et al., 2015).

3.5 Potential mechanisms for the change in ice nucleation ability

3.5.1 $(NH_4)_2SO_4$ addition

The contribution to particle surface area of Us-dust by illite, quartz, chlorite, kaolinite, and feldspar was 37%, 24%, 23%, 12%, and 5%, respectively. In Us-dust, only about 13% of feldspar type particles have K element (i.e., K-feldspar-like) and the rest was Na/Ca-feldspar (Fig. S6). Previous studies have shown that the K-feldspar exhibits higher IMF activity than Na/Ca-feldspar (Atkinson et al., 2013; Harrison et al., 2016; Peckhaus et al., 2016; Whale et al., 2017; Zolles et al., 2015). Although K-feldspar-like particles accounted for only a small fraction of Us-dust surface area, the ΔT_{50}^{u} values were comparable to those reported for K-feldspar, suggesting that feldspar may provide a disproportionate contribution to the highly active sites responsible for the observed enhancement as compared with S-dust. However, K-feldspar alone could not fully account the enhancement at AS/Dust mass ratio greater than 1 (Fig. 7c, d), implying contributions from other minerals (e.g., kaolinite) in Us-dust.

NH_4^+ in solution can replace the K^+ on the surface of K-feldspar, forming interfacial sites that promote ice nucleation (Worthy et al., 2021). In addition, NH_4^+ adsorbed on dust surfaces may alter the arrangement and orientation of water molecules, potentially enhancing ice nucleation activity (Anim-Danso et al., 2016; Kumar et al., 2018; Worthy et al., 2021). At the pH (~5.5–6.6) of droplets with AS, the surfaces of feldspar (point of zero charge (PZC) < 2), quartz (PZC ≈ 2), and kaolinite (PZC ≈ 3–6) were all negatively charged and can adsorb NH_4^+ due to the lack of charge-balancing cations (Kumar et al., 2018, 2019a; Worthy et al., 2021). ΔT_{50}^{u} of Us-dust exhibited a Boltzmann-type (sigmoidal) dependence on AS concentration, suggesting that the enhancement is consistent a threshold-saturation interfacial process from low to high

AS coverage on dust surface (Fig.7c, d). Our experimental data are consistent with NH_4^+ adsorption on mineral surface being an important mechanism contributing to the ice nucleation enhancement by AS. The ice nucleation enhancement on Us-dust by AS observed here may involve NH_4^+ adsorption on the dust surface, while other mechanisms, such as the participation of NH_4^+ in ion exchange on feldspar (Worthy et al., 2021) and regulation of hydrogen bond ordering at dust surface (Whale, 2022), may also contribute the observed enhancement.

3.5.2 NaCl addition

Previous studies have shown that the effect of near-neutral alkali salt solutions on the IMF of mineral dust depends on the particle type and their surface properties (Kumar et al., 2018, 2019a, b; Whale et al., 2018). Suppression of the IMF on feldspar by NaCl may be attributed additional surface process beyond colligative behavior, in which NaCl can increase the interfacial free energy to form ice cluster (Whale et al., 2018). Kumar et al. (2018) suggested that alkali cations may adsorb onto negatively charged mineral surface and form an interfacial double layer on feldspar that block ice nucleation sites. In contrast, Perkins et al. (2020) showed that NaCl solution has no effect on the IMF activity of ATD (Fig.8b). Similarly, no significant change in T_{50} was observed for Us-dust in this study at NaCl concentration from 5×10^{-4} M to 5×10^{-2} M (Fig.8b). However, N_s of Us-dust at warmer temperature (258 K–262 K) gradually decrease with increasing NaCl concentration, indicating selective suppression of the most ice active sites (Fig.8e). Because feldspar tends to respond more strongly to NaCl suppression (Whale et al., 2018) and is highly active at warm temperatures (Atkinson et al., 2013; Boose et al., 2019), the observed high sensitivity of Us-dust to NaCl above 258 K are likely associated with feldspar. At lower temperatures, non-feldspar minerals, which is less sensitive to NaCl than feldspar (Fig.8b), control the freezing of Us-dust.

3.5.3 Acid treatment

Previous studies have found that the effect of acid treatments on IMF of mineral dust is sample dependent. Suppression on the IMF activity of feldspar and ATD by H_2SO_4 treatment was linked to acid-driven surface reactions, loss of surface K^+, and formation of sulfate-containing products on particle surface (Augustin-Bauditz et al., 2014;

Kumar et al., 2018; Niedermeier et al., 2011). For HNO_3, HCl, and organic acid treatment, Yun et al. (2021) proposed that the reduced IMF ability of K-rich feldspar was associated with H_3O^+/K^+ exchange and incongruent dissolution of Al and Si. Sullivan et al. (Sullivan et al., 2010b) found that HNO_3 did not significantly suppress the freezing by ATD above water saturation. However, Perkins et al. (2020) showed that acid treatment on ATD affected the nucleation sites at warm temperatures, while ice active sites at low temperatures remain unaffected. For Us-dust, no significant shift in ΔT_{50}^{u} was observed after treatment with H_2SO_4 (2.5×10^{-4} M to 2.5×10^{-2} M) or HNO_3 (5×10^{-4} M to 5×10^{-2} M), indicating that limited impact on IMF activity in terms of T_{50}. However, above 258 K, N_s of Us-dust was reduced by HNO_3 at 5×10^{-2} M and H_2SO_4 at all tested concentrations, but was slightly enhanced by HNO_3 at 5×10^{-4} M and 5×10^{-3} M. These imply that acids have effects on nucleation sites of Us-dust at warmer temperatures, but direction and magnitude are dependent on acid type and concentration.

3.5.4 Heat treatment

In this study, heat treatment was used to examine changes in IMF activity and the potential thermal deactivation of labile ice active sites. Previous studies have shown that heat treatment either suppress the IMF ability of ATD or exerts no effect. Niedermeier et al. (2011) reported that the IMF activity of ATD remined unchanged after heating. Perkins et al. (2020) found stronger heating caused larger changes in freezing behaver of ATD. They suggested that ice active sites at warmer temperatures are more sensitive to heating, which may be associated with defects, heat sensitive components, or other labile sites on the ATD surface. In addition, Pereira et al. (2022) reported reduced the IMF ability of agricultural soil dust after heating which was attributed to heat sensitive components, like organic matter. In our study, heat treatment on Us-dust at 95°C for 30 min reduced ice nucleation activity (N_s) at warm temperatures, whereas activity at lower temperatures was largely retained. This response is consistent with Perkins et al. (2020), suggesting that ice active sites in complex dust samples differ in thermal sensitivity. The preferential loss of activity at warmer temperatures suggests the deactivation of thermally labile ice active sites, which may be intrinsic to the mineral dust itself or associated with heat sensitive components, including biological

materials or organic matter. However, the specific origins of these labile ice active sites were not determined here and require further investigation. Heat treatment experiments were not conducted on S-dust; therefore, whether sonication influences the thermal sensitivity of dust INPs remains uncertain.

3.6 Heterogeneous ice nucleation rate coefficient

The experimentally derived J_{het} and its parameterizations as functions of Δa_w and temperature are presented in Fig.9 and Fig. S7, respectively. Us-dust nucleated ice starting from relatively low Δa_w (~0.08) and high temperature (i. e., 264 K) at the investigated concentrations. The temperature and Δa_w dependence of J_{het} for Us-dust is substantially steeper than for S-dust. This is associated with the differences in particle size and composition before and after ultrasonic treatment (Section 3.1). AS enhanced the J_{het} of Us-dust more progressively with AS concentration. Only minor variations in J_{het} for Us-dust (i.e., less than one order of magnitude) were observed above 258 K after heat, acid (H_2SO_4 and HNO_3), and NaCl treatments (Fig. S7). J_{het} of Us-dust is a few orders of magnitude higher than kaolinite and illite, but lower than Aluminum oxide and Iron oxide at the investigated Δa_w (Fig. 9c). Compared with non-mineral or biological substances, in terms of J_{het} (Fig. 9d), Us-dust is less efficient than fungal spores (Iannone et al., 2011), comparable to 1-nonadecanol (Knopf and Forrester, 2011), but more efficient than marine microbes (*Thalassiosira Pseudonana* and *Nannochloris Atomus*) (Alpert et al., 2011; Knopf et al., 2011), and humic like substances (leonardite and Pahokee Peat) (Rigg et al., 2013). After mixed with AS, J_{het} for Us-dust shifted toward but still lower than aluminum oxide, iron oxide, and fungal spores.

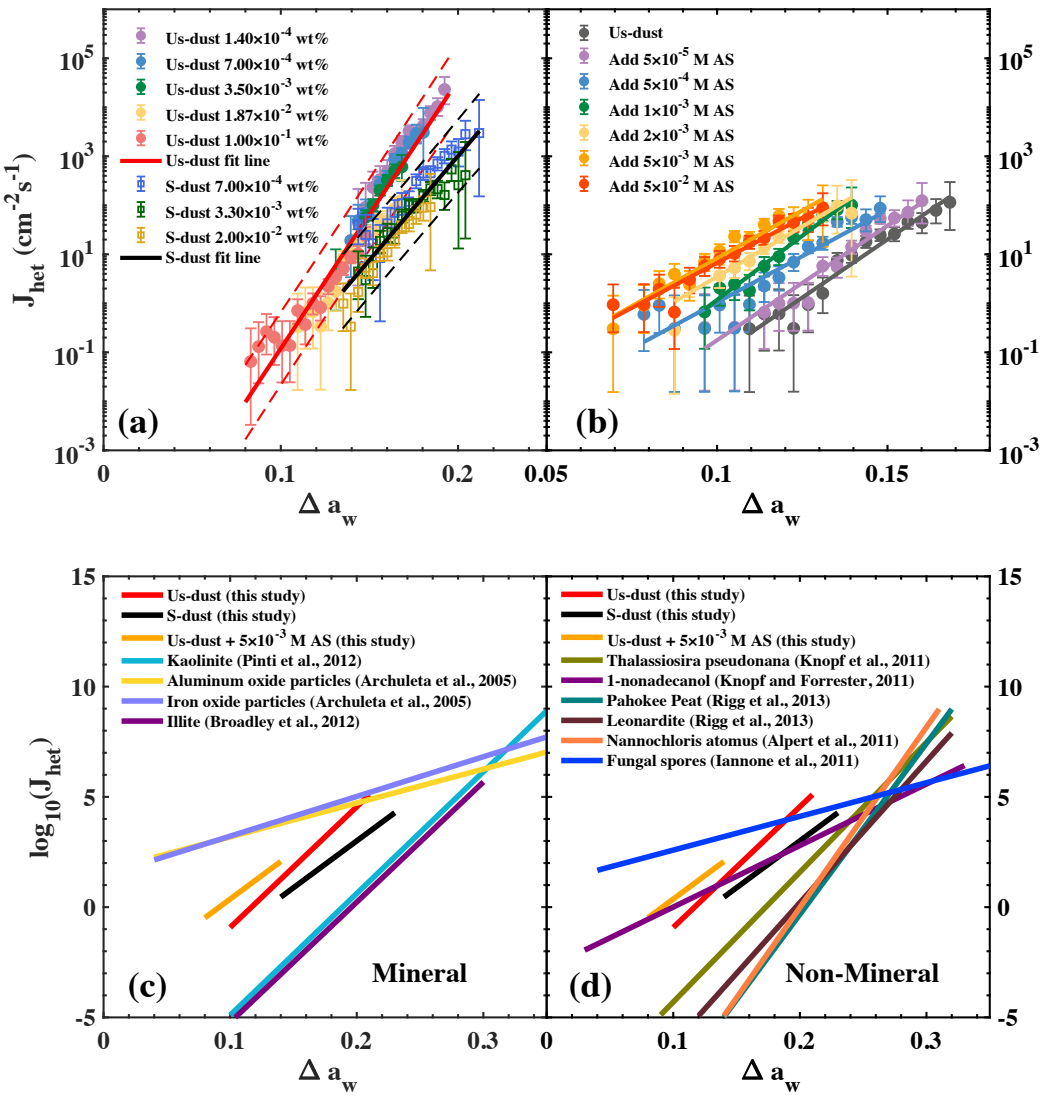

Figure 9. J_{het} as a function of Δa_w for Us-dust and S-dust (a), and Us-dust (1.87×10^{-2} wt%) mixed with AS (b). Comparison J_{het} of Us-dust, S-dust, and Us-dust mixed with 0.005 M AS with minerals (c) and non-minerals (d) from previous studies (Alpert et al., 2011; Archuleta et al., 2005; Broadley et al., 2012; Iannone et al., 2011; Knopf et al., 2002, 2011; Knopf and Alpert, 2013; Knopf and Forrester, 2011; Murray et al., 2011; Pinti et al., 2012; Rigg et al., 2013). Dashed lines (a) are the 95% prediction intervals. Solid lines (a, b) are parameterizations according to $\log(J_{het}) = m_2 \times \Delta a_w + n_2$ and the values of m_2 and n_2 are listed in Table S2.

4. Atmospheric implication: impact of AS on IMF by Tengger Desert dust

As desert dust is emitted into the atmosphere and transported over long distances to different environments or high altitude, it may be aged and mixed with AS. The effect

on the IMF activity by AS should be represented in parameterizations and considered in cloud modeling. Including AS concentration as another variable, we proposed parameterizations of N_s and J_{het} to consider the impact of AS on IMF of Us-dust. Parameterizations as a function of AS to dust mass ratio (AS/Dust, r) and temperature (T) or Δa_w were developed as follows:

$$N_s = 10^{(k_1 \times T + B_1)}, \tag{8}$$

$$J_{het} = 10^{(k_2 \times T + B_2)}, \tag{9}$$

$$J_{het} = 10^{(k_3 \times \Delta a_w + B_3)}, \tag{10}$$

where the parameters B (B_1, B_2, and B_3) are fitted by a Boltzmann sigmoid function, $B = a + \frac{b}{\left(1+e^{\frac{\log_{10}(r)+c}{d}}\right)}$. The fitting parameters are listed in Table 2. Evaluation of N_s (T, r), J_{het} (T, r), and J_{het} (Δa_w, r) parameterizations against the experimental observations is shown in Figs. S8-S10. The proposed parameterizations reproduce the observed impacts of AS on the IMF ability of Us-dust at the investigated AS and dust concentrations (AS < 0.1M, AS/Dust = 0.03~30).

We applied the proposed parameterizations for Tengger Desert dust internally mixed with AS to estimate their N_s and J_{het} under representative atmospheric conditions. As shown in Fig. 10, Both N_s and J_{het} increase markedly with decreasing temperature (increasing Δa_w) and with increasing AS/Dust mass ratio, consistent with the observed AS enhancement on IMF activity. As an illustrative case, an AS particle with an initial diameter of 0.5 μm takes up water and grows into a 10 μm droplet, corresponding to an AS concentration of about 0.002 M. When a Tengger Desert dust particle (0.5 μm and 10^{-13} g) is incorporated into this 10 μm AS droplet (AS/Dust of 1.16), the parameterizations predict N_s of 2.17×10^6 cm^{-2} and J_{het} of 24.55 cm^{-2} s^{-1} at 260 K. Under these conditions, Δa_w is 0.12. J_{het} value determined from J_{het} (Δa_w, r) parameterization is 23.96 cm^{-2} s^{-1}, consistent with the value calculated by J_{het} (T, r) parameterization. In contrast, the corresponding N_s, J_{het} (Δa_w), and J_{het} (T) for untreated Tengger Desert dust is 5.30×10^4 cm^{-2}, 0.76 cm^{-2} s^{-1}, and 0.90 cm^{-2} s^{-1} at 260 K, respectively, about 30-40 times lower than dust mixed with AS. This example suggests that internal mixing with AS can substantially increase the contribution of Tengger Desert dust to IMF under

atmospherically relevant conditions.

The parameterizations developed here link dust IMF properties to AS loading and to temperature or Δa_w, providing a practical means to predict AS driven changes in IMF activity. N_s (T, r) can be combined with dust particle surface area to estimate INP concentrations under the singular hypothesis, while J_{het} (T, r) and J_{het} (Δa_w, r) can be used in time-dependent freezing frameworks to predict INP production rates. These parameterizations based on measurements of the Tengger Desert dust are constrained by AS concentrations below 0.1 M.

Table 2 The k, a, b, c, and d values for parameterizations of N_s (T, r), J_{het} (T, r), and J_{het} (Δa_w, r) along with Eqs.8-10 for Tengger Desert dust mixed with AS.

Parametric formula	N_s **(**T**,** r**)**	J_{het} **(**T**,** r**)**	J_{het} **(**Δa_w**,**r**)**
k	-0.39	-0.38	41.17
a	106.45	100.73	-3.07
LCL_a	105.71	100.39	-3.22
UCL_a	107.19	101.07	-2.93
b	1.82	-1.68	-1.56
LCL_b	0.77	-2.29	-1.82
UCL_b	2.87	-1.07	-1.31
c	-0.26	-0.20	-0.21
LCL_c	-0.74	-0.51	-0.35
UCL_c	0.22	0.10	-0.08
d	-0.36	0.36	0.35
LCL_d	-0.88	0.04	0.21
UCL_d	0.15	0.68	0.49
$RMSE$	0.22	0.24	0.24
R^2	0.93	0.91	0.91

Note: the parameter k was determined through a grid search that minimizes the sum of absolute errors.

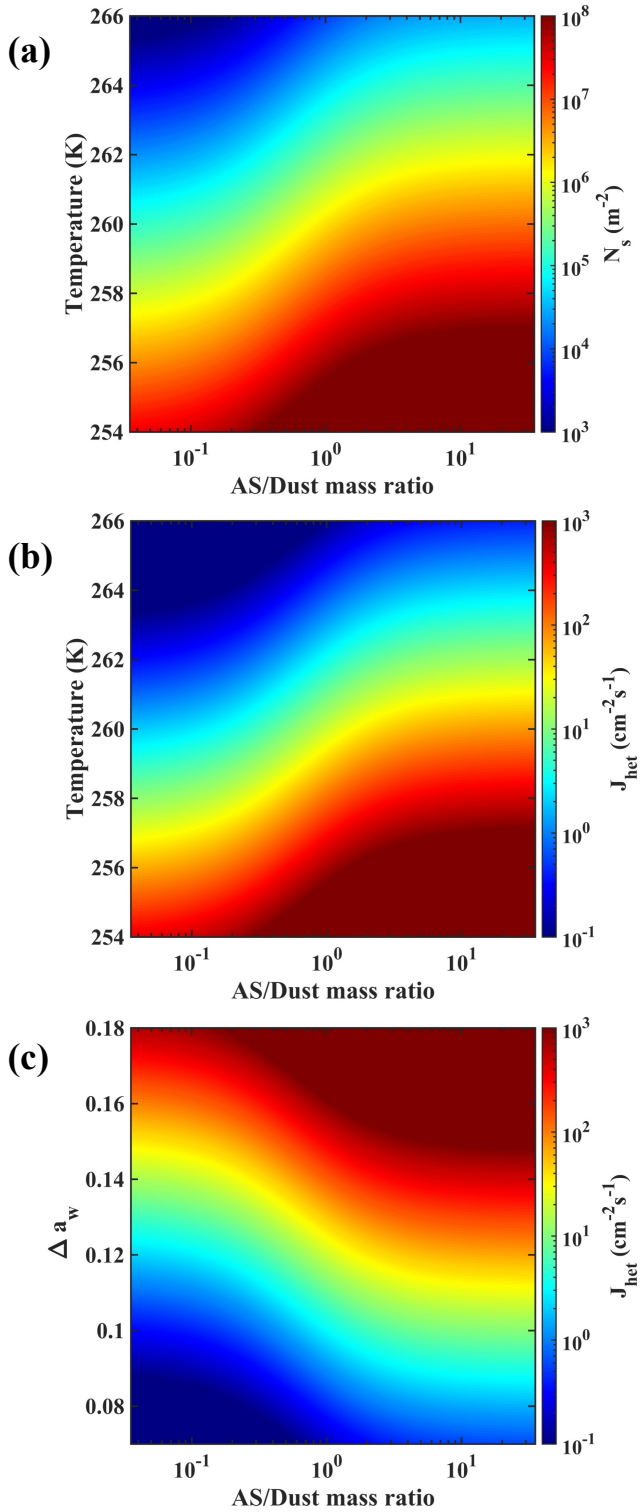

Figure 10. Prediction of N_s and J_{het} based on the parameterization of Us-dust mixed with AS. (a) N_s and (b) J_{het} as a function of temperature and AS/Dust mass ratio, (c) J_{het} as a function of Δa_w and AS/Dust mass ratio.

5. Conclusion

We investigated the IMF of surface-collected dust from Tengger Desert and its response to various aging treatments, including mixing with NaCl and AS, heating, and acid treatment with H_2SO_4 and HNO_3. Tengger Desert dust initiated the IMF at temperatures as high as 264.3 K, with T_{50} increased from 253.6 K to 258.5 K as the dust mass fraction rose from 1.4×10^{-4} wt% to 1.0×10^{-1} wt%. Single particle analysis showed that ultrasonic treatment of dust in water substantially modified the suspended dust population. The ultrasonic treatment shifted the modal particle diameter from approximately 0.35 to 0.7 μm and altered mineralogical composition with increased contributions from chlorite, illite, and feldspar, reduced kaolinite, and minor change in quartz. The 2% increase in particle surface area of feldspar may contribute to the approximately 2 K higher T_{50} and one order of magnitude increase in N_s. This result suggests that mineralogical composition of complex natural dust can strongly influence ice nucleation properties, especially when it contains components with high ice nucleation activity.

Among the investigated aging treatments, AS enhanced the ice nucleation activity of Us-dust. When AS changed from 5×10^{-5} M to 5×10^{-2} M, the increase in T_{50} for Us-dust at 1.87×10^{-2} wt% changed from 0.4 K to 4.7 K. The corresponding increments in T_{50}, as well as N_s and J_{het}, followed a Boltzmann sigmoidal response. This supports the possibility that NH_4^+ adsorption on mineral surface and the associated activation of ice active sites may be an important mechanism for the ice nucleation enhancement by AS. Other treatments on Us-dust by NaCl, acid (H_2SO_4 and HNO_3), and heating have minor impacts on the IMF behavior in terms of T_{50}. However, heat and H_2SO_4 treatments, as well as higher concentrations of NaCl and HNO_3 (>2.5×10^{-2} M), led to a reduction in N_s above 258 K, whereas lower concentrations of NaCl (5×10^{-4} M) and HNO_3 (< 5×10^{-3} M) produced modest increases. These results indicate the presence of labile ice active sites at warmer temperatures with variably sensitive to chemical and thermal processing. Ice nucleation modeling studies should consider these effects by NaCl, H_2SO_4 and HNO_3.

This study provided experimental constraints on the IMF properties of Tengger Desert

dust for the modeling assessments on the impacts of East Asian dust to mixed-phase cloud formation. Parameterizations of the experimentally derived $N_s(T)$ and $J_{het}(T$ or $\Delta a_w)$ of desert dust were proposed. N_s of Us-dust was comparable to those reported for feldspar and showed stronger temperature dependence than previously reported desert dust. Although N_s were broadly comparable to East Asian airborne dust below 260 K, Tengger Desert dust were a few orders of magnitude lower than commonly used parameterizations for desert dust of Niemand et al. (2012) and Ullrich et al. (2017) above 260 K. J_{het} of Us-dust was higher than those reported for kaolinite, illite, some marine microorganisms, and humic-like substances, but was lower than aluminum oxide, iron oxide, and fungal spores. Considering the impact of AS, we proposed parameterizations of N_s (T, r), J_{het} (T, r), and J_{het} (a_w, r) as a function of the mass ratio of AS/Dust (r). These parameterizations illustrate how experimentally derived changes in dust ice nucleation associated with AS aging can be represented in a model framework. However, they are constrained by experiments using a single dust source and aging protocol, and this study primarily investigated the effects of inorganic aging on the IMF activity. Future studies should investigate the effects of organic compounds and other atmospheric aging processes on dust ice nucleation. Further experiments and ice nucleation parameterizations involving dust from different sources and a wider range of atmospheric aging conditions are needed to evaluate their broader applicability in cloud models.

Data availability. All data are given in the main text or in the Supplement.

Supplement. The supplement related to this article is available online.

Author contributions. JX wrote the first draft of the manuscript. SKW, HYQ, SLC, YJZ, and QW performed the experiments. YY set up the ice nucleation experimental system. JX, SKW, JYL, YWH, and TZ performed the data analysis. YHC collected the samples. BBW, DFZ, and YHC initiated the study. BBW supervised the project. BBW and JX led the discussion and all authors contributed to the data interpretation and the manuscript writing.

Competing interests. At least one of the (co-)authors is a member of the editorial

board of *Atmospheric Chemistry and Physics.*

Acknowledgements. JYL and TZ acknowledge the support by PhD Fellowship of State Key Laboratory of Marine Environmental Science (MEL), Xiamen University. QW acknowledges the support by MEL Summer Undergraduate Research Fellowship Program. We thank Lisi Zhao for the sample preparation. CCSEM/EDX analysis was done at user facility of Center of Major Equipment and Technology (COMET) at Xiamen University.

Financial support. This research has been supported by National Natural Science Foundation of China (42375069, 41775133, 42075076, 42576033), Shanghai Key Laboratory of Ocean-land-atmosphere Boundary Dynamics and Climate Change, and State Key Laboratory of Marine Environmental Science at Xiamen University Internal Program (MELRI2002).

Reference:

Alpert, P. A., Aller, J. Y., and Knopf, D. A.: Ice nucleation from aqueous NaCl droplets with and without marine diatoms, Atmos. Chem. Phys., 11, 5539–5555, https://doi.org/10.5194/acp-11-5539-2011, 2011.

Alpert, P. A., Kilthau, W. P., O'Brien, R. E., Moffet, R. C., Gilles, M. K., Wang, B., Laskin, A., Aller, J. Y., and Knopf, D. A.: Ice-nucleating agents in sea spray aerosol identified and quantified with a holistic multimodal freezing model, Sci. Adv., 8, 1–11, https://doi.org/10.1126/sciadv.abq6842, 2022.

Anim-Danso, E., Zhang, Y., and Dhinojwala, A.: Surface charge affects the structure of interfacial ice, J. Phys. Chem. C, 120, 3741–3748, https://doi.org/10.1021/acs.jpcc.5b08371, 2016.

Archuleta, C. M., DeMott, P. J., and Kreidenweis, S. M.: Ice nucleation by surrogates for atmospheric mineral dust and mineral dust/sulfate particles at cirrus temperatures, Atmos. Chem. Phys., 5, 2617–2634, https://doi.org/10.5194/acp-5-2617-2005, 2005.

Atkinson, J. D., Murray, B. J., Woodhouse, M. T., Whale, T. F., Baustian, K. J., Carslaw, K. S., Dobbie, S., O'Sullivan, D., and Malkin, T. L.: The importance of feldspar for ice nucleation by mineral dust in mixed-phase clouds, Nature, 498, 355–358, https://doi.org/10.1038/nature12278, 2013.

Augustin-Bauditz, S., Wex, H., Kanter, S., Ebert, M., Niedermeier, D., Stolz, F., Prager, A., and Stratmann, F.: The immersion mode ice nucleation behavior of mineral dusts: a comparison of different pure and surface modified dusts, Geophys. Res. Lett., 41, 7375–7382, https://doi.org/10.1002/2014GL061317, 2014.

Baker, M. B.: Cloud microphysics and climate, Science, 276, 1072–1078,

https://doi.org/10.1126/science.276.5315.1072, 1997.

Boose, Y., Welti, A., Atkinson, J., Ramelli, F., Danielczok, A., Bingemer, H. G., Plötze, M., Sierau, B., Kanji, Z. A., and Lohmann, U.: Heterogeneous ice nucleation on dust particles sourced from nine deserts worldwide – Part 1: Immersion freezing, Atmos. Chem. Phys., 16, 15075–15095, https://doi.org/10.5194/acp-16-15075-2016, 2016.

Boose, Y., Baloh, P., Plötze, M., Ofner, J., Grothe, H., Sierau, B., Lohmann, U., and Kanji, Z. A.: Heterogeneous ice nucleation on dust particles sourced from nine deserts worldwide – Part 2: Deposition nucleation and condensation freezing, Atmos. Chem. Phys., 19, 1059–1076, https://doi.org/10.5194/acp-19-1059-2019, 2019.

Broadley, S. L., Murray, B. J., Herbert, R. J., Atkinson, J. D., Dobbie, S., Malkin, T. L., Condliffe, E., and Neve, L.: Immersion mode heterogeneous ice nucleation by an illite rich powder representative of atmospheric mineral dust, Atmos. Chem. Phys., 12, 287–307, https://doi.org/10.5194/acp-12-287-2012, 2012.

Burrows, S. M., McCluskey, C. S., Cornwell, G., Steinke, I., Zhang, K., Zhao, B., Zawadowicz, M., Raman, A., Kulkarni, G., China, S., Zelenyuk, A., and DeMott, P. J.: Ice-nucleating particles that impact clouds and climate: observational and modeling research needs, Rev. Geophys., 60, e2021RG000745, https://doi.org/10.1029/2021RG000745, 2022.

Chen, J., Wu, Z., Chen, J., Reicher, N., Fang, X., Rudich, Y., and Hu, M.: Size-resolved atmospheric ice-nucleating particles during East Asian dust events, Atmos. Chem. Phys., 21, 3491–3506, https://doi.org/10.5194/acp-21-3491-2021, 2021.

Chen, J., Xu, J., Wu, Z., Meng, X., Yu, Y., Ginoux, P., DeMott, P. J., Xu, R., Zhai, L., Yan, Y., Zhao, C., Li, S.-M., Zhu, T., and Hu, M.: Decreased dust particles amplify the cloud cooling effect by regulating cloud ice formation over the Tibetan Plateau, Sci. Adv., 10, eado0885, https://doi.org/10.1126/sciadv.ado0885, 2024.

China, S., Alpert, P. A., Zhang, B., Schum, S., Dzepina, K., Wright, K., Owen, R. C., Fialho, P., Mazzoleni, L. R., Mazzoleni, C., and Knopf, D. A.: Ice cloud formation potential by free tropospheric particles from long-range transport over the Northern Atlantic Ocean, J. Geophys. Res.: Atmos., 122, 3065–3079, https://doi.org/10.1002/2016JD025817, 2017.

Cziczo, D. J., Froyd, K. D., Hoose, C., Jensen, E. J., Diao, M., Zondlo, M. A., Smith, J. B., Twohy, C. H., and Murphy, D. M.: Clarifying the dominant sources and mechanisms of cirrus cloud formation, Science, 340, 1320–1324, https://doi.org/10.1126/science.1234145, 2013.

DeMott, P. J., Sassen, K., Poellot, M. R., Baumgardner, D., Rogers, D. C., Brooks, S. D., Prenni, A. J., and Kreidenweis, S. M.: African dust aerosols as atmospheric ice nuclei, Geophys. Res. Lett., 30, 1732, https://doi.org/10.1029/2003GL017410, 2003.

DeMott, P. J., Prenni, A. J., McMeeking, G. R., Sullivan, R. C., Petters, M. D., Tobo, Y., Niemand, M., Möhler, O., Snider, J. R., Wang, Z., and Kreidenweis, S. M.: Integrating laboratory and field data to quantify the immersion freezing ice nucleation activity of mineral dust particles, Atmos. Chem. Phys., 15, 393–409, https://doi.org/10.5194/acp-15-393-2015, 2015.

Diehl, K., Debertshäuser, M., Eppers, O., Schmithüsen, H., Mitra, S. K., and Borrmann, S.: Particle surface area dependence of mineral dust in immersion freezing mode: investigations with freely

suspended drops in an acoustic levitator and a vertical wind tunnel, Atmos. Chem. Phys., 14, 12343–12355, https://doi.org/10.5194/acp-14-12343-2014, 2014.

Eastwood, M. L., Cremel, S., Wheeler, M., Murray, B. J., Girard, E., and Bertram, A. K.: Effects of sulfuric acid and ammonium sulfate coatings on the ice nucleation properties of kaolinite particles, Geophys. Res. Lett., 36, 1–5, https://doi.org/10.1029/2008GL035997, 2009.

Hader, J. D., Wright, T. P., and Petters, M. D.: Contribution of pollen to atmospheric ice nuclei concentrations, Atmos. Chem. Phys., 14, 5433–5449, https://doi.org/10.5194/acp-14-5433-2014, 2014.

Harrison, A. D., Whale, T. F., Carpenter, M. A., Holden, M. A., Neve, L., O'Sullivan, D., Vergara Temprado, J., and Murray, B. J.: Not all feldspars are equal: a survey of ice nucleating properties across the feldspar group of minerals, Atmos. Chem. Phys., 16, 10927–10940, https://doi.org/10.5194/acp-16-10927-2016, 2016.

Hoose, C. and Möhler, O.: Heterogeneous ice nucleation on atmospheric aerosols: A review of results from laboratory experiments, Atmos. Chem. Phys., 12, 9817–9854, https://doi.org/10.5194/acp-12-9817-2012, 2012.

Hu, T., Wu, F., Song, Y., Liu, S., Duan, J., Zhu, Y., Cao, J., and Zhang, D.: Morphology and mineralogical composition of sandblasting dust particles from the Taklimakan Desert, Sci. Total Environ., 834, 155315, https://doi.org/10.1016/j.scitotenv.2022.155315, 2022.

Iannone, R., Chernoff, D. I., Pringle, A., Martin, S. T., and Bertram, A. K.: The ice nucleation ability of one of the most abundant types of fungal spores found in the atmosphere, Atmos. Chem. Phys., 11, 1191–1201, https://doi.org/10.5194/acp-11-1191-2011, 2011.

Iwata, A. and Matsuki, A.: Characterization of individual ice residual particles by the single droplet freezing method: a case study in the Asian dust outflow region, Atmos. Chem. Phys., 18, 1785–1804, https://doi.org/10.5194/acp-18-1785-2018, 2018.

Kandler, K., Benker, N., Bundke, U., Cuevas, E., Ebert, M., Knippertz, P., Rodríguez, S., Schütz, L., and Weinbruch, S.: Chemical composition and complex refractive index of Saharan Mineral Dust at Izaña, Tenerife (Spain) derived by electron microscopy, Atmos. Environ., 41, 8058–8074, https://doi.org/10.1016/j.atmosenv.2007.06.047, 2007.

Kanji, Z. A., Welti, A., Chou, C., Stetzer, O., and Lohmann, U.: Laboratory studies of immersion and deposition mode ice nucleation of ozone aged mineral dust particles, Atmos. Chem. Phys., 13, 9097–9118, https://doi.org/10.5194/acp-13-9097-2013, 2013.

Kanji, Z. A., Ladino, L. A., Wex, H., Boose, Y., Burkert-Kohn, M., Cziczo, D. J., and Krämer, M.: Overview of ice nucleating particles, Meteorol. Monogr., 58, 1.1-1.33, https://doi.org/10.1175/AMSMONOGRAPHS-D-16-0006.1, 2017.

Kaufmann, L., Marcolli, C., Hofer, J., Pinti, V., Hoyle, C. R., and Peter, T.: Ice nucleation efficiency of natural dust samples in the immersion mode, Atmos. Chem. Phys., 16, 11177–11206, https://doi.org/10.5194/acp-16-11177-2016, 2016.

Kawai, K. and Matsui, H.: Contributions of dust source regions to ice nucleating particles in mixed-phase clouds simulated with a global climate–aerosol model, J. Clim., 38, 4925–4939, https://doi.org/10.1175/JCLI-D-24-0696.1, 2025.

Kawai, K., Matsui, H., and Tobo, Y.: High potential of Asian dust to act as ice nucleating particles in mixed-phase clouds simulated with a global aerosol-climate model, J. Geophys. Res.: Atmos., 126, e2020JD034263, https://doi.org/10.1029/2020JD034263, 2021.

Knopf, D. A. and Alpert, P. A.: A water activity based model of heterogeneous ice nucleation kinetics for freezing of water and aqueous solution droplets, Faraday Discuss., 165, 513–534, https://doi.org/10.1039/c3fd00035d, 2013.

Knopf, D. A. and Alpert, P. A.: Atmospheric ice nucleation, Nat. Rev. Phys., 5, 203–217, https://doi.org/10.1038/s42254-023-00570-7, 2023.

Knopf, D. A. and Forrester, S. M.: Freezing of water and aqueous NaCl droplets coated by organic monolayers as a function of surfactant properties and water activity, J. Phys. Chem. A, 115, 5579–5591, https://doi.org/10.1021/jp2014644, 2011.

Knopf, D. A. and Lopez, M. D.: Homogeneous ice freezing temperatures and ice nucleation rates of aqueous ammonium sulfate and aqueous levoglucosan particles for relevant atmospheric conditions, Phys. Chem. Chem. Phys., 11, 8056–8068, https://doi.org/10.1039/b903750k, 2009.

Knopf, D. A., Koop, T., Luo, B. P., Weers, U. G., and Peter, T.: Homogeneous nucleation of NAD and NAT in liquid stratospheric aerosols: insufficient to explain denitrification, Atmos. Chem. Phys., 2, 207–214, https://doi.org/10.5194/acp-2-207-2002, 2002.

Knopf, D. A., Alpert, P. A., Wang, B., and Aller, J. Y.: Stimulation of ice nucleation by marine diatoms, Nat. Geosci., 4, 88–90, https://doi.org/10.1038/ngeo1037, 2011.

Knopf, D. A., Alpert, P. A., Wang, B., O'Brien, R. E., Kelly, S. T., Laskin, A., Gilles, M. K., and Moffet, R. C.: Microspectroscopic imaging and characterization of individually identified ice nucleating particles from a case field study, J. Geophys. Res.: Atmos., 119, 10365–10381, https://doi.org/10.1002/2014JD021866, 2014.

Knopf, D. A., Alpert, P. A., and Wang, B.: The role of organic aerosol in atmospheric ice nucleation: A review, ACS Earth Space Chem., 2, 168–202, https://doi.org/10.1021/acsearthspacechem.7b00120, 2018.

Koop, T. and Zobrist, B.: Parameterizations for ice nucleation in biological and atmospheric systems, Phys. Chem. Chem. Phys., 11, 10839–10850, https://doi.org/10.1039/b914289d, 2009.

Koop, T., Luo, B., Biermann, U. M., Crutzen, P. J., and Peter, T.: Freezing of HNO_3 H_2SO_4 H_2O solutions at stratospheric temperatures: nucleation statistics and experiments, J. Phys. Chem. A, 101, 1117–1133, https://doi.org/10.1021/jp9626531, 1997.

Koop, T., Ng, H. P., Molina, L. T., and Molina, M. J.: A new optical technique to study aerosol phase transitions: the nucleation of ice from H_2SO_4 aerosols, J. Phys. Chem. A, 102, 8924–8931, https://doi.org/10.1021/jp9828078, 1998.

Koop, T., Luo, B., Tsias, A., and Peter, T.: Water activity as the determinant for homogeneous ice nucleation in aqueous solutions, Nature, 406, 611–614, https://doi.org/10.1038/35020537, 2000.

Kulkarni, G., Zhang, K., Zhao, C., Nandasiri, M., Shutthanandan, V., Liu, X., Fast, J., and Berg, L.: Ice formation on nitric acid-coated dust particles: Laboratory and modeling studies, J. Geophys. Res.: Atmos., 120, 7682–7698, https://doi.org/10.1002/2014JD022637, 2015.

Kumar, A., Marcolli, C., Luo, B., and Peter, T.: Ice nucleation activity of silicates and aluminosilicates in pure water and aqueous solutions – Part 1: The K-feldspar microcline, Atmos. Chem. Phys., 18, 7057–7079, https://doi.org/10.5194/acp-18-7057-2018, 2018.

Kumar, A., Marcolli, C., and Peter, T.: Ice nucleation activity of silicates and aluminosilicates in pure water and aqueous solutions – Part 2: Quartz and amorphous silica, Atmos. Chem. Phys., 19, 6035–6058, https://doi.org/10.5194/acp-19-6035-2019, 2019a.

Kumar, A., Marcolli, C., and Peter, T.: Ice nucleation activity of silicates and aluminosilicates in pure water and aqueous solutions – Part 3: Aluminosilicates, Atmos. Chem. Phys., 19, 6059–6084, https://doi.org/10.5194/acp-19-6059-2019, 2019b.

Ladino Moreno, L. A., Stetzer, O., and Lohmann, U.: Contact freezing: A review of experimental studies, Atmos. Chem. Phys., 13, 9745–9769, https://doi.org/10.5194/acp-13-9745-2013, 2013.

Laskin, A., Iedema, M. J., and Cowin, J. P.: Quantitative time-resolved monitoring of nitrate formation in sea salt particles using a CCSEM/EDX single particle analysis, Environ. Sci. Technol., 36, 4948–4955, https://doi.org/10.1021/es020551k, 2002.

Li, J., Liu, W., Castarède, D., Gu, W., Li, L., Ohigashi, T., Zhang, G., Tang, M., Thomson, E. S., Hallquist, M., Wang, S., and Kong, X.: Hygroscopicity and ice nucleation properties of dust/salt mixtures originating from the source of East Asian dust storms, Front. Environ. Sci., 10, 897127, https://doi.org/10.3389/fenvs.2022.897127, 2022.

Link, N., Removski, N., Yun, J., Fleming, L. T., Nizkorodov, S. A., Bertram, A. K., and Al-Abadleh, H. A.: Dust-catalyzed oxidative polymerization of catechol and its impacts on ice nucleation efficiency and optical properties, ACS Earth Space Chem., 4, 1127–1139, https://doi.org/10.1021/acsearthspacechem.0c00107, 2020.

Lohmann, U. and Feichter, J.: Global indirect aerosol effects: A review, Atmos. Chem. Phys., 5, 715–737, https://doi.org/10.5194/acp-5-715-2005, 2005.

Menut, L., Siour, G., Bessagnet, B., Couvidat, F., Journet, E., Balkanski, Y., and Desboeufs, K.: Modelling the mineralogical composition and solubility of mineral dust in the Mediterranean area with CHIMERE 2017r4, Geosci. Model Dev., 13, 2051–2071, https://doi.org/10.5194/gmd-13-2051-2020, 2020.

Möhler, O., Benz, S., Saathoff, H., Schnaiter, M., Wagner, R., Schneider, J., Walter, S., Ebert, V., and Wagner, S.: The effect of organic coating on the heterogeneous ice nucleation efficiency of mineral dust aerosols, Environ. Res. Lett., 3, 025007, https://doi.org/10.1088/1748-9326/3/2/025007, 2008.

Murray, B. J., Broadley, S. L., Wilson, T. W., Atkinson, J. D., and Wills, R. H.: Heterogeneous freezing of water droplets containing kaolinite particles, Atmos. Chem. Phys., 11, 4191–4207, https://doi.org/10.5194/acp-11-4191-2011, 2011.

Murray, B. J., O'Sullivan, D., Atkinson, J. D., and Webb, M. E.: Ice nucleation by particles immersed in supercooled cloud droplets, Chem. Soc. Rev., 41, 6519–6554, https://doi.org/10.1039/c2cs35200a, 2012.

Niedermeier, D., Hartmann, S., Clauss, T., Wex, H., Kiselev, A., Sullivan, R. C., DeMott, P. J., Petters, M. D., Reitz, P., Schneider, J., Mikhailov, E., Sierau, B., Stetzer, O., Reimann, B., Bundke,

U., Shaw, R. A., Buchholz, A., Mentel, T. F., and Stratmann, F.: Experimental study of the role of physicochemical surface processing on the IN ability of mineral dust particles, Atmos. Chem. Phys., 11, 11131–11144, https://doi.org/10.5194/acp-11-11131-2011, 2011.

Niemand, M., Möhler, O., Vogel, B., Vogel, H., Hoose, C., Connolly, P., Klein, H., Bingemer, H., DeMott, P., Skrotzki, J., and Leisner, T.: A particle-surface-area-based parameterization of immersion freezing on desert dust particles, J. Atmos. Sci., 69, 3077–3092, https://doi.org/10.1175/JAS-D-11-0249.1, 2012.

Peckhaus, A., Kiselev, A., Hiron, T., Ebert, M., and Leisner, T.: A comparative study of K-rich and Na/Ca-rich feldspar ice-nucleating particles in a nanoliter droplet freezing assay, Atmos. Chem. Phys., 16, 11477–11496, https://doi.org/10.5194/acp-16-11477-2016, 2016.

Pereira, D. L., Gavilán, I., Letechipía, C., Raga, G. B., Puig, T. P., Mugica-Álvarez, V., Alvarez-Ospina, H., Rosas, I., Martinez, L., Salinas, E., Quintana, E. T., Rosas, D., and Ladino, L. A.: Mexican agricultural soil dust as a source of ice nucleating particles, Atmos. Chem. Phys., 22, 6435–6447, https://doi.org/10.5194/acp-22-6435-2022, 2022.

Perkins, R. J., Gillette, S. M., Hill, T. C. J., and DeMott, P. J.: The labile nature of ice nucleation by Arizona Test Dust, ACS Earth Space Chem., 4, 133–141, https://doi.org/10.1021/acsearthspacechem.9b00304, 2020.

Pinti, V., Marcolli, C., Zobrist, B., Hoyle, C. R., and Peter, T.: Ice nucleation efficiency of clay minerals in the immersion mode, Atmos. Chem. Phys., 12, 5859–5878, https://doi.org/10.5194/acp-12-5859-2012, 2012.

Pruppacher, H. R. and Klett, J. D.: Microphysics of clouds and precipitation, 2nd edn., Kluwer Academic Publishers, Dordrecht, 954 pp., 1997.

Reicher, N., Budke, C., Eickhoff, L., Raveh-Rubin, S., Kaplan-Ashiri, I., Koop, T., and Rudich, Y.: Size-dependent ice nucleation by airborne particles during dust events in the eastern Mediterranean, Atmos. Chem. Phys., 19, 11143–11158, https://doi.org/10.5194/acp-19-11143-2019, 2019.

Reischel, M. T. and Vali, G.: Freezing nucleation in aqueous electrolytes, Tellus A: Dyn. Meteorol. Oceanogr., 27, 414–427, https://doi.org/10.3402/tellusa.v27i4.9989, 1975.

Rigg, Y., Alpert, P., and Knopf, D.: Immersion freezing of water and aqueous ammonium sulfate droplets initiated by humic-like substances as a function of water activity, Atmos. Chem. Phys., 13, 6603–6622, https://doi.org/10.5194/acp-13-6603-2013, 2013.

Rosenfeld, D., Sherwood, S., Wood, R., and Donner, L.: Climate effects of aerosol-cloud interactions, Science, 343, 379–380, https://doi.org/10.1126/science.1247490, 2014.

Shi, Y. and Liu, X.: Dust radiative effects on climate by glaciating mixed-phase clouds, Geophys. Res. Lett., 46, 6128–6137, https://doi.org/10.1029/2019GL082504, 2019.

Storelvmo, T.: Aerosol effects on climate via mixed-phase and ice clouds, Annu. Rev. Earth Planet. Sci., 45, 199–222, https://doi.org/10.1146/annurev-earth-060115-012240, 2017.

Sullivan, R. C., Miñambres, L., DeMott, P. J., Prenni, A. J., Carrico, C. M., Levin, E. J. T., and Kreidenweis, S. M.: Chemical processing does not always impair heterogeneous ice nucleation of mineral dust particles, Geophys. Res. Lett., 37, L24805, https://doi.org/10.1029/2010GL045540,

2010a.

Sullivan, R. C., Petters, M. D., DeMott, P. J., Kreidenweis, S. M., Wex, H., Niedermeier, D., Hartmann, S., Clauss, T., Stratmann, F., Reitz, P., Schneider, J., and Sierau, B.: Irreversible loss of ice nucleation active sites in mineral dust particles caused by sulphuric acid condensation, Atmos. Chem. Phys., 10, 11471–11487, https://doi.org/10.5194/acp-10-11471-2010, 2010b.

Tobo, Y., DeMott, P. J., Raddatz, M., Niedermeier, D., Hartmann, S., Kreidenweis, S. M., Stratmann, F., and Wex, H.: Impacts of chemical reactivity on ice nucleation of kaolinite particles: A case study of levoglucosan and sulfuric acid, Geophys. Res. Lett., 39, L19803, https://doi.org/10.1029/2012GL053007, 2012.

Ullrich, R., Hoose, C., Möhler, O., Niemand, M., Wagner, R., Höhler, K., Hiranuma, N., Saathoff, H., and Leisner, T.: A new ice nucleation active site parameterization for desert dust and soot, J. Atmos. Sci., 74, 699–717, https://doi.org/10.1175/JAS-D-16-0074.1, 2017.

Vali, G.: Quantitative evaluation of experimental results on the heterogeneous freezing nucleation of supercooled liquids, J. Atmos. Sci., 28, 402–409, https://doi.org/10.1175/1520-0469(1971)028%3C0402:QEOERA%3E2.0.CO;2, 1971.

Vali, G., DeMott, P. J., Möhler, O., and Whale, T. F.: Technical note: A proposal for ice nucleation terminology, Atmos. Chem. Phys., 15, 10263–10270, https://doi.org/10.5194/acp-15-10263-2015, 2015.

Wang, B., Laskin, A., Roedel, T., Gilles, M. K., Moffet, R. C., Tivanski, A. V., and Knopf, D. A.: Heterogeneous ice nucleation and water uptake by field-collected atmospheric particles below 273 K, J. Geophys. Res.: Atmos., 117, D00V19, https://doi.org/10.1029/2012JD017446, 2012.

Wang, W., Shao, L., Zhang, D., Li, Y., Li, W., Liu, P., and Xing, J.: Mineralogical similarities and differences of dust storm particles at Beijing from deserts in the north and northwest, Sci. Total Environ., 803, 149980, https://doi.org/10.1016/j.scitotenv.2021.149980, 2022.

Whale, T. F.: Disordering effect of the ammonium cation accounts for anomalous enhancement of heterogeneous ice nucleation, J. Chem. Phys., 156, 144503, https://doi.org/10.1063/5.0084635, 2022.

Whale, T. F., Murray, B. J., O'Sullivan, D., Wilson, T. W., Umo, N. S., Baustian, K. J., Atkinson, J. D., Workneh, D. A., and Morris, G. J.: A technique for quantifying heterogeneous ice nucleation in microlitre supercooled water droplets, Atmos. Meas. Tech., 8, 2437–2447, https://doi.org/10.5194/amt-8-2437-2015, 2015.

Whale, T. F., Holden, M. A., Kulak, A. N., Kim, Y.-Y., Meldrum, F. C., Christenson, H. K., and Murray, B. J.: The role of phase separation and related topography in the exceptional ice-nucleating ability of alkali feldspars, Phys. Chem. Chem. Phys., 19, 31186–31193, https://doi.org/10.1039/C7CP04898J, 2017.

Whale, T. F., Holden, M. A., Wilson, T. W., O'Sullivan, D., and Murray, B. J.: The enhancement and suppression of immersion mode heterogeneous ice-nucleation by solutes, Chem. Sci., 9, 4142–4151, https://doi.org/10.1039/C7SC05421A, 2018.

Wilson, P. W. and Haymet, A. D. J.: Effect of solutes on the heterogeneous nucleation temperature of supercooled water: An experimental determination, Phys. chem. chem. phys.: PCCP, 11, 2679–

2682, https://doi.org/10.1039/b817585c, 2009.

Worthy, S. E., Kumar, A., Xi, Y., Yun, J., Chen, J., Xu, C., Irish, V. E., Amato, P., and Bertram, A. K.: The effect of $(NH_4)_2SO_4$ on the freezing properties of non-mineral dust ice-nucleating substances of atmospheric relevance, Atmos. Chem. Phys., 21, 14631–14648, https://doi.org/10.5194/acp-21-14631-2021, 2021.

Wright, T. P., Petters, M. D., Hader, J. D., Morton, T., and Holder, A. L.: Minimal cooling rate dependence of ice nuclei activity in the immersion mode, J. Geophys. Res.: Atmos., 118, 10535–10543, https://doi.org/10.1002/jgrd.50810, 2013.

Xue, J., Zhang, T., Park, K., Yan, J., Yoon, Y. J., Park, J., and Wang, B.: Diverse sources and aging change the mixing state and ice nucleation properties of aerosol particles over the western Pacific and Southern Ocean, Atmos. Chem. Phys., 24, 7731–7754, https://doi.org/10.5194/acp-24-7731-2024, 2024.

Yao, Y., Alpert, P. A., Zuend, A., and Wang, B.: Does liquid–liquid phase separation impact ice nucleation in mixed polyethylene glycol and ammonium sulfate droplets?, Phys. Chem. Chem. Phys., 25, 80–95, https://doi.org/10.1039/D2CP04407B, 2023.

Yun, J., Kumar, A., Removski, N., Shchukarev, A., Link, N., Boily, J.-F., and Bertram, A. K.: Effects of inorganic acids and organic solutes on the ice nucleating ability and surface properties of potassium-rich feldspar, ACS Earth Space Chem., 5, 1212–1222, https://doi.org/10.1021/acsearthspacechem.1c00034, 2021.

Zhang, C., Wu, Z., Chen, J., Chen, J., Tang, L., Zhu, W., Pei, X., Chen, S., Tian, P., Guo, S., Zeng, L., Hu, M., and Kanji, Z. A.: Ice-nucleating particles from multiple aerosol sources in the urban environment of Beijing under mixed-phase cloud conditions, Atmos. Chem. Phys., 22, 7539–7556, https://doi.org/10.5194/acp-22-7539-2022, 2022.

Zhao, L., Xue, J., Wang, S., Tian, P., Huang, M., Bi, K., and Wang, B.: Single particle characteristics and ice nucleation potential of particles collected during Asian dust storms in 2021, Sci. Total Environ., 948, 174829, https://doi.org/10.1016/j.scitotenv.2024.174829, 2024.

Zobrist, B., Koop, T., Luo, B. P., Marcolli, C., and Peter, T.: Heterogeneous ice nucleation rate coefficient of water droplets coated by a nonadecanol monolayer, J. Phys. Chem. C, 111, 2149–2155, https://doi.org/10.1021/jp066080w, 2007.

Zobrist, B., Marcolli, C., Peter, T., and Koop, T.: Heterogeneous ice nucleation in aqueous solutions: the role of water activity, J. Phys. Chem. A, 112, 3965–3975, https://doi.org/10.1021/jp7112208, 2008.

Zolles, T., Burkart, J., Häusler, T., Pummer, B., Hitzenberger, R., and Grothe, H.: Identification of ice nucleation active sites on feldspar dust particles, J. Phys. Chem. A, 119, 2692–2700, https://doi.org/10.1021/jp509839x, 2015.